

# Perspective: Magnon-magnon coupling in hybrid magnonics

Wei Zhang,<sup>1,\*</sup> Yuzan Xiong,<sup>1</sup> Jia-Mian Hu,<sup>2</sup> Joseph Sklenar,<sup>3</sup> Mitra Mani Subedi,<sup>3</sup> M.Benjamin Jungfleisch,<sup>4</sup> Vinayak S. Bhat,<sup>4</sup> Yi Li,<sup>5</sup> Luqiao Liu,<sup>6</sup> Qiuyuan Wang,<sup>6</sup> Yunqiu Kelly Luo,<sup>7</sup> Youn Jue Bae,<sup>8</sup> and Benedetta Flebus<sup>9</sup>

<sup>1</sup>*Department of Physics and Astronomy, University of North Carolina at Chapel Hill, Chapel Hill, NC 27599, USA*

<sup>2</sup>*Department of Materials Science and Engineering,*

*University of Wisconsin-Madison, Madison, Wisconsin, 53706, USA*

<sup>3</sup>*Department of Physics and Astronomy, Wayne State University, Detroit, MI 48202, USA*

<sup>4</sup>*Department of Physics and Astronomy, University of Delaware, Newark, DE 19716, USA*

<sup>5</sup>*Materials Science Division, Argonne National Laboratory, Argonne, IL 60439, USA*

<sup>6</sup>*Department of Electrical Engineering and Computer Science,*

*Massachusetts Institute of Technology, Cambridge, Massachusetts 02139, USA*

<sup>7</sup>*Department of Physics and Astronomy, Department of Chemistry,*

*Mork Family Department of Chemical Engineering and Materials Science,*

*University of Southern California, Los Angeles, CA, 90089 USA*

<sup>8</sup>*Department of Chemistry and Chemical Biology, Cornell University, Ithaca, NY, 14850, USA*

<sup>9</sup>*Department of Physics, Boston College, 140 Commonwealth Avenue Chestnut Hill, Massachusetts 02467, USA*

## ABSTRACT

The internal coupling of magnetic excitations (magnons) with themselves has created a new research sub-field in hybrid magnonics, i.e., magnon-magnon coupling, which focuses on materials discovery and engineering for probing and controlling magnons in a coherent manner. This is enabled by, one, the abundant mechanisms of introducing magnetic interactions, with examples of exchange coupling, dipolar coupling, RKKY coupling, and DMI coupling, and two, the vast knowledge of how to control magnon band structure, including field and wavelength dependences of frequencies, for determining the degeneracy of magnon modes with different symmetries. In particular, we discuss how magnon-magnon coupling is implemented in various materials systems, with examples of magnetic bilayers, synthetic antiferromagnets, nanomagnetic arrays, layered van der Waals magnets, and (DMI SOT materials) in magnetic multilayers. We then introduce new concept of applications for these hybrid magnonic materials systems, with examples of frequency up/down conversion and magnon-exciton coupling, and discuss what properties are desired for achieving those applications.

## INTRODUCTION

Hybrid solid-state systems play an important role in experimental and theoretical condensed matter physics. They harness interacting excitations, such as sound waves (phonons), microwave (MW) and light waves (photons), and quantum defects (spin color centers) to complete tasks that are beyond the capability of each individual system [1, 2]. Recent development in quantum science has put such hybrid systems to the forefront of condensed matter physics research, calling for upgraded benchmark performance in the efficient, coherent, and robust transformation of information carried by these fundamental excitations.

Spin waves (or magnons), have received increased attention in such hybrid quantum systems due to their small wavelength, dissipationless transport, nonlinearity, GHz-THz resonance frequency, and notably, the ability to hybridize with a wide variety of other quasiparticles and light waves, hence the concept of “hybrid magnonics” [5–9]. To date, strong and coherent couplings between magnons and other excitations, such as microwave photons, light photons, phonons, single spins, and qubits, have been demonstrated. Consequently, the field of hybrid magnonics has grown and developed into different ramifications, such as magnon-photon, magnon-

phonon, and magnon-light coupling systems, etc, presenting a broad spectrum of coherent phenomena, including but not limited to, level repulsion/attraction [10–14], magnetically-induced transparency(MIT) [15–17], super/ultrastrong couplings [18], pump-induced nonlinearity [19–23], zero-reflection(ZR) [24, 25], and spectrum singularities [26–28], bestowing emerging quantum engineering functionalities [2, 6–9].

In hybrid magnonics, so far, most attention has been focused in hybridizing magnons with another excitation of distinct nature, i.e., Magnon +  $X$ , with the goal of developing energy and signal transduction functionalities across different physical platforms and coherent information processing in an artificial two-level system. For example, treating the hybrid system as an analogous “two-level” system in the sense of the Jaynes–Cummings Hamiltonian, the Rabi process shuffles the two-level states in an analogous Bloch sphere representation, shown in Fig. 1. On the magnon side, the Kittel (wavevector  $\mathbf{k} = 0$ ) mode, being the most prominent and zero-th order, was often exploited, see Fig. 1. However, introducing finite- $\mathbf{k}$  modes may bring in further advantages, such as using the wavevector  $\mathbf{k}$  as a state variable, leveraging the full magnon dispersion, and integrating the magnon precessional phase ( $\phi$ ) as a control parameter into the technologically important Ramsey process. Computational demonstration of such a “magnonic Ramsey process” has recently been reported in magnon-photon systems [4] using protocols that are similar to classical-domain demonstration of the Ramesy

\* All correspondance should be addressed to: zhwei@unc.edu

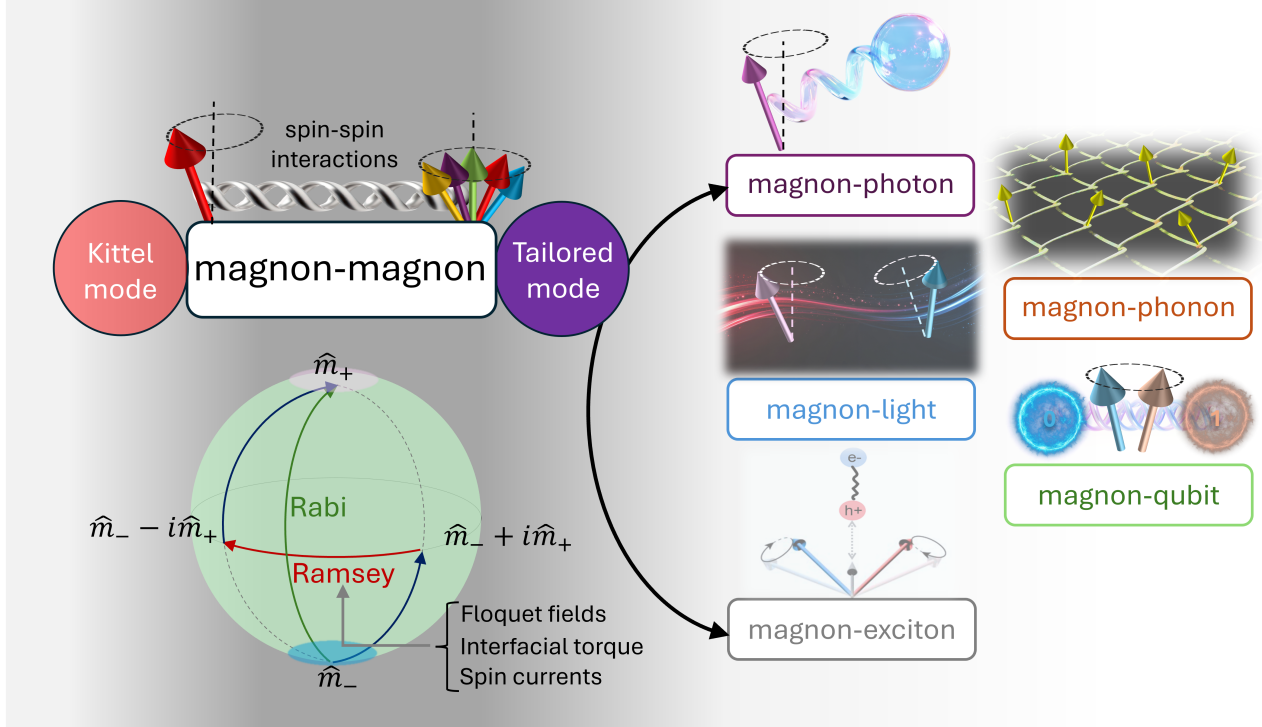


FIG. 1. The field of hybrid magnonics has grown and developed into different ramifications, such as magnon-photon, magnon-phonon, and magnon-light coupling systems, with the goal of developing energy and signal transduction functionalities across different physical platforms. The magnon-magnon coupling is presented as a unique and versatile approach towards inducing and tailoring magnon modes with desirable properties for further hybridization in the various hybrid magnonic contexts, i.e. Magnon +  $X$ . The Bloch sphere representation shows how hybrid magnonics can perform coherent information processing, e.g. Rabi oscillation and Ramsey interference, as analogous to a two-level system [3, 4]. The symbols  $\hat{m}_+$  and  $\hat{m}_-$  represent some generic single magnon modes (states).

process in a two-level photonic system [3]. Such a scheme can be also extended to magnon-magnon coupled systems between two generic single magnon modes ( $\hat{m}_+$  and  $\hat{m}_-$ ), in which additional, novel control schemes can be introduced, including interface exchange, spin current (spin torque), and Floquet field, due to both subsystems being “magnonic” in nature.

On the other hand, underpinning the Magnon +  $X$  hybridization is the fundamental versatile “spin-couplings” manifesting magneto-optical, magneto-electric, and magneto-strictive effects [2]. Besides the cross-platform Magnon +  $X$  hybridizations, one distinct advantage of magnons is their strong/coherent interaction among themselves – the magnon-magnon coupling – providing a unique route towards generation of novel, tailored magnon modes [15, 29–43]. Such magnon-magnon interaction underpins a diverse range of coherent phenomena that are governed by spin-spin interactions, including but not limited to, direct exchange [44], Ruderman–Kittel–Kasuya–Yosida (RKKY) [45], and Dzyaloshinskii–Moriya interaction (DMI) [46, 47]. The different symmetries in these couplings can be synergistically combined to generate, modulate, and detect unconventional mode forms in a Magnon +  $X$  hybrid, thereby providing tailored magnon modes as further

candidates for multi-partite, cross-platform hybridizations as illustrated in Fig. 1. Specifically, integrating magnon-magnon coupling in the Magnon +  $X$  process offers several derived advantages, as summarized in Fig. 2, Keys 1 – 6:

1. *Wavelength-selectivity:* the interfacial spin couplings can be highly localized, hence allowing effective excitation of short-wavelength magnon modes down to the deep-exchange magnon regime [15, 16, 18, 30, 31, 33, 48]. Such an interfacial spin perturbation scheme is analogous to the excitation of coherent THz magnons in ferromagnet thin films by current-induced interfacial spin torques [49–51].

2. *Superimposing spin-spin interactions:* the various spin-coupling types, direct-Ex, RKKY, dipolar, and DMI, entail different symmetries and controlling parameters. Therefore, they can be synergistically engineered to interfere, constructively or destructively for selective mode excitations [52–57]. For example, in a canonical magnon-magnon coupled Permalloy/YIG bilayer structure, it has recently been shown [25] that the phase of magnetization precession at the interface is collectively controlled by both the Zeeman torque (from the microwave drive) and the interlayer exchange torque. Such a dual-channel excitation scheme provides a new knob

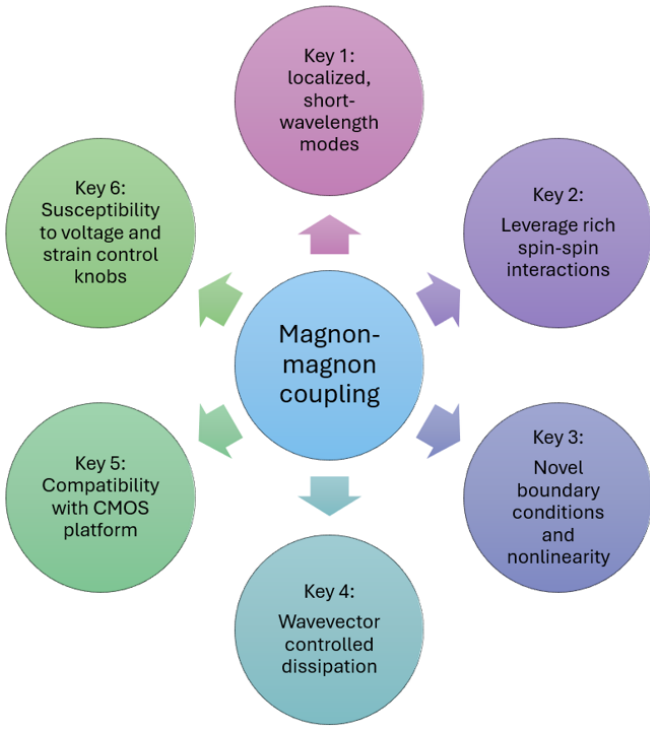


FIG. 2. The various key attributes of magnon-magnon coupling in the context of hybrid magnonics.

to control both the phase and magnetization amplitude of the individual exchange magnon modes in the YIG film, suggesting new opportunities in the realm of phase-controlled hybrid magnonics.

3. *Novel boundary conditions and strong nonlinearity*: beyond the extended, pristine films, new boundary conditions to the excited magnon modes can be imposed by nano-structuring (such as in the cases of artificial spin-ice and magnonic crystals) [58, 59], interfacing with other layers [60], additional current injections [61], and mutual spin pumping [33, 62], hence allowing to leverage the rich collective magnonic dispersions and their high tunability [21, 63–67]. Besides, the strong nonlinearity of magnonics can be used to enrich hybrid magnon modes, leading to finite mode-overlap of different magnon modes that are presumed to be orthogonal in the linear regime. Examples include the recently discovered pump-induced mode anticrossing arising from the three-magnon scattering [19, 22], opto-electro-magnonic oscillator due to nonlinear magnon-photon coupling [21], and coherent magnon mode generation in the nonlinear excitation regime [63–67].

4. *Dissipation(damping) control*: magnon-magnon coupling can modify effective magnetic damping of a mode through mutual spin pumping, especially when two modes are at same or nearly same frequencies (i.e. at co-resonance or near co-resonance condition), which offers two major benefits: (i) reducing energy loss, which can increase the distance waves can travel and hence improve

energy efficiency, and (ii) strengthening or weakening (selectively) specific modes, which can be used to stabilize useful oscillations while filtering unwanted ones. These capabilities would be highly valuable for spintronic and magnonic device applications. For example, by controlling the damping of individual modes electrical control of magnon frequencies in the vicinity of an avoided energy level crossing is enabled [33, 62, 68–72].

5. *Engineering scalability*: magnon coupling involves, more often than not, magnetic films and multilayers on planar substrates (including wafers), a modular component that shares the same physical form factor and packing model as those of silicon, thus is reconcilable with the needs for scaling with state-of-the-art CMOS architectures, as opposed to conventional resonator platforms like YIG spheres and 3D cavities. Recent advances in magnonics also advocate a scheme shift from large magnetic volumes to nanoscale lithographic structures, to realize miniaturization and true CMOS compatibility rather than relying on stand-alone bulk resonators. Concrete progress has already aligned with the CMOS style footprints. For instance, fully planar lithographic demonstrations show reconfigurable magnon-magnon coupling in ultrathin insulators under a spin-orbit torque control: Pt nanostripes patterned atop 3-nm Bi-doped YIG define on-chip magnonic cavities whose modes hybridize with boundary magnons, yielding a tunable anticrossing gap and enabling electrical on/off control of the coupling [73]. The compact, planar geometry supports multiple cavities and engineerable inter-cavity couplings, the kind of footprint that naturally maps to CMOS packaging. As efficient magnon-based computing blocks have been experimentally demonstrated, with the additional versatility provided by magnon-magnon coupling, a hybrid computing architecture with additional functionality and/or efficiency can be anticipated [73–75].

6. *Compatible with mature spintronic/magnetic control knobs*: since hybrid magnon-magnon coupling can be achieved with interfacial coupling in magnetic thin-film bilayers [33, 34, 67, 68, 73, 76, 77], conventional mature spintronic and magnetic control toolkits, such as spin-transfer torque [78], spin-orbit torque [79], strain control [80] and voltage control [81], can be directly adopted for engineering magnon-magnon couplings. However, the main engineering bottleneck remains the magnon electron transducer. The efficiency of the usual conversion routes based on microwave antennas for excitation and spin pumping with inverse spin Hall readout is low. This limits the density of addressable circuits at the chip level [74]. A promising route is the magnetoelectric transducer that combines piezoelectric and magnetostrictive elements. This approach is driven by ac voltage and is expected to be far more energy efficient than any current-driven antennas. In optimized cells the projected operation can reach the atto-joule energy scale [73].

It is natural to expect that a growing ability to tune magnon-magnon interactions will reorient the role of spintronic systems – adding new research thrusts atop

predominantly application-driven goals toward their use as platforms for exploring emergent phenomena of fundamental interest. For instance, the programmable control over dispersion and hybridization of synthetic antiferromagnets (syn-AFMs) [82], whose collective spin-wave modes can be systematically reconfigured through interlayer exchange, anisotropy, and symmetry-breaking fields, draws a natural parallel to how metamaterials have been used to access novel regimes of dynamics and topology [83, 84]. As both the coherent and incoherent of their long-wavelength behavior is well understood, magnon-magnon coupled syn-AFMs might offer accessible framework for investigating the emergence of non-Hermitian phenomena that have been attracting so much attention in recent years [85].

From a fundamental point of view, magnonic systems provide a rare—though largely unexplored—opportunity to directly test the resilience of non-Hermitian dynamics in the presence of strong intrinsic nonlinearities [86, 87], an aspect largely inaccessible in other platforms. At the same time, the application of these principles may also unlock new functionalities, such as reconfigurable spintronic diodes based on nonreciprocal spin-wave transport—particularly as progress continues in engineering chiral interactions within magnetic heterostructures [88].

Another intriguing, yet still underexplored, in magnonic systems is Floquet engineering [89], where periodic driving can induce new modes, topological band structures, or symmetry-selective coupling. While synthetic antiferromagnets offer a natural setting for this approach [67], equally promising are the discrete spin-wave modes that arise in laterally confined magnetic structures, which can serve as building blocks for implementing synthetic dimensions or dynamically tunable coupling networks [90, 91]. Together, these examples highlight just a few of the opportunities that become accessible as magnon-magnon interactions are brought under experimental control, suggesting that a broad and largely untapped landscape of driven, correlated, and topologically structured magnonic phenomena lies within reach.

## MAGNON-MAGNON COUPLING ENABLED BY DIFFERENT TYPES OF SPIN-SPIN INTERACTIONS

Below, we review the subject based on the different types of spin-spin interactions pertinent to each magnon-magnon system category, a comprehensive list of material examples can be found in Table I.

### Interfacial exchange coupling in magnetic bilayers

The study of coherent dynamic coupling between two adjacent magnetic layers was among the earliest explorations of coherent magnon-magnon coupling, motivated primarily by the question of how to efficiently ex-

cite short-wavelength exchange spin waves. Usually, one needs to create a spatially nonuniform microwave field to achieve geometrical overlap with the spin wave, enabling their coupling and energy exchange. This typically was done by fabricating nanoscale microwave antennas, which, however, further reduces coupling efficiency due to the narrow antenna electrodes.

*a. Metal-insulator system* In 2018, Klinger *et al.* [30], Chen *et al.* [31], and Qin *et al.* [32] reported the excitation of the perpendicular standing spin wave (PSSW) mode—an exchange spin wave mode with a wave vector perpendicular to the thin film plane—in a YIG film, assisted by an adjacent ferromagnetic (FM) layer, see Fig.3 (c-e). By growing the FM layer on top of YIG film, interfacial exchange coupling (dipolar coupling in Chen *et al.*'s work) enables coherent magnetic excitation transfer from the FM layer to YIG [Fig.3 (a)]. Since the selected FM materials (Co, Ni, or CoFeB) have much larger magnetization compared to YIG, the in-plane field dependence of their Kittel modes exhibits different  $\omega - H$  slopes, allowing one mode to intersect with the other due to the PSSW frequency offset in YIG [Fig.3(b), (f)]. Moreover, because the Kittel mode in the FM layer efficiently couples with a uniform microwave rf field, the spatially nonuniform PSSW mode in YIG can be excited by the uniform microwave field through its interfacial interaction with the FM layer, making it easily observable experimentally. Without this technique, the PSSW mode barely couples to the uniform microwave field, with the amplitude of the  $n = 1$  PSSW mode being 50 times weaker than that of the uniform mode [92].

Another significant consequence of these experiments is the observation of magnon mode hybridization between the FM and YIG layers, which has a profound impact in their application in coherent information processing [2, 6]. This demonstrates that magnon excitations can be coherently exchanged between the two spatially separated magnetic systems, enabling a highly compact, solid-state hybrid magnonic system with a nanometer-scale total vertical stacking, in complementary to their lateral dimensions. Since the coupling originates from the interfacial interaction between the two magnetic layers, the magnetic bilayer hybrid magnonic system allows for structural engineering along the lateral dimensions without affecting the properties of mode hybridization [97, 98], allowing room for integrating with additional designs and constructions at the chip level.

Figure 4 summarizes the various geometries for magnon-magnon coupling investigations, pertinent to different types of magnon modes of interest. The left column [Fig.4(a,b,c)] shows uniform, extended bilayer coupling in which the thickness of the film defines the magnonic cavity. The situation applies to both insulator/metal [Fig.4(b)] and all-insulator [Fig.4(c)] systems. The middle column [Fig.4(d,e,f)] exemplifies the device geometry in which an FM stripe (via lithography, etc) couples locally to an extended YIG film. In this case, the magnon-magnon coupling leverages both the direct ex-

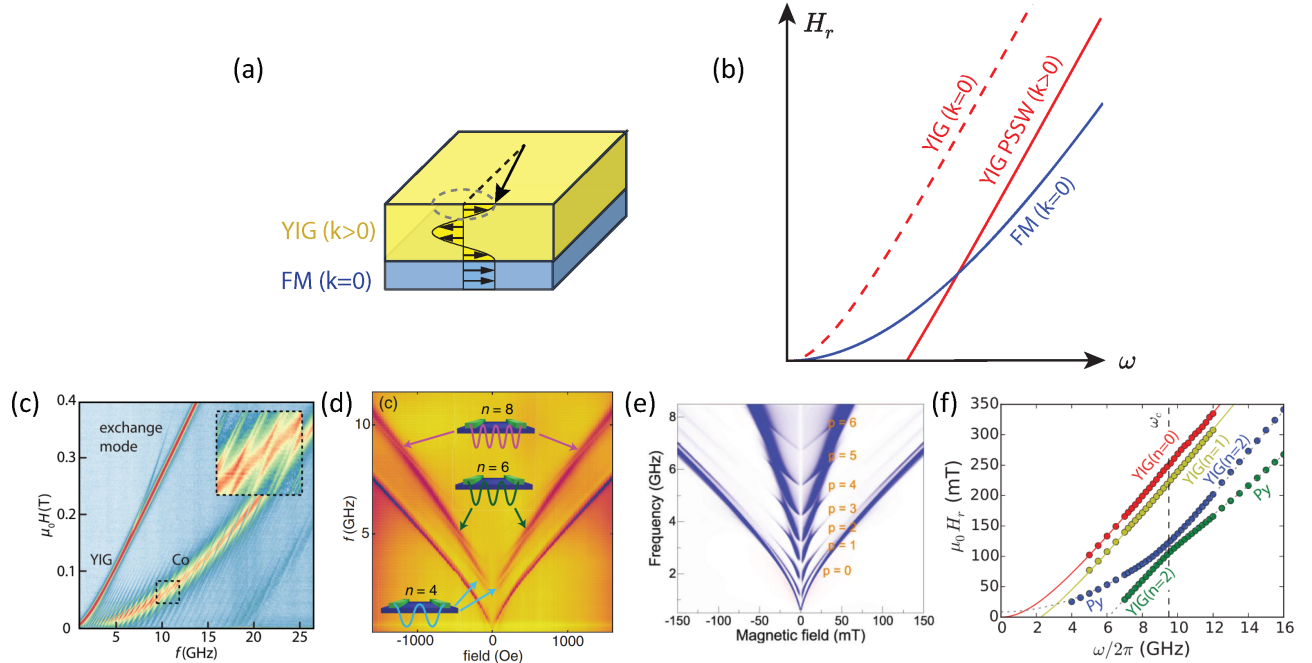


FIG. 3. (a) Schematic of coupled magnon-magnon dynamics in a YIG/FM bilayer mediated by interfacial exchange coupling, with uniform mode ( $k = 0$ ) excited in the FM layer and the perpendicular standing spin wave mode ( $k > 0$ ) excited in the YIG layer. (b)  $H_r$ - $\omega$  dependence for the YIG PSSW mode (red) and the FM uniform mode (blue) that intersect with each other. YIG uniform mode is also shown in red dashed curve. (c-f) Coherent magnon-magnon coupling in (c) YIG/Co [30], (d) YIG/Ni[31], (e) YIG/CoFeB[32] and (f) YIG/NiFe[33].

change coupling (at the interface) and an enhanced dipolar interaction (due to micro- or nano-structuring). The locally excited magnon modes (at and below the center stripe), instead of being confined by a cavity, can propagate along the lateral sides, and be detected via dc rectifications, e.g., using spin Hall effect of Pt, as in Fig.4(e), rf inductive antennas, or magneto-optical probes, see Fig.4(f). Further, the right column [Fig.4(g,h,i)] exemplifies the construction of a lateral magnonic cavity by using pairs of FM stripe(s). In such a case, the magnon modes are confined not only vertically but also laterally defined by the dimensions of the cavity, which can be easily controlled by the location of the stripe(s). Notably, the FM stripes can also serve as complementary, local antennas, as in Fig.4(h), apart from being the cavity boundaries; or else, they can be used only to define the cavity boundaries while the excitation is globally sourced by an external rf structure (e.g. a waveguide beneath).

*b. Coupling strengths* The interfacial exchange coupling provides an interlayer magnon-magnon coupling strength ( $g_c$ ) which can be derived analytically from the Landau-Lifshitz-Gilbert equation, as derived by Li *et al.*[33]:

$$g_c \simeq \sqrt{\frac{J}{M_1 t_1} \frac{J}{M_2 t_2}} \quad (1)$$

Here,  $J$  is the interfacial coupling energy density between the two magnetic layers, while  $M_{1,2}$ ,  $t_{1,2}$  represent the magnetization and the thickness of the two layers, respec-

tively. Note that there is a pre-factor in Eq.1 which comes from the ellipticity of magnetization precession and is close to one [33]. Eq. 1 shows that the interlayer magnon-magnon coupling comes from a mutual interaction of the two layers, and their coupling strength is the geometric average of the effective interfacial exchange field, which is inversely proportional to the magnetization and thin film thickness. This is similar to the coupling strength in magnon-photon coupling, where the coupling strength is inversely proportional to the square root of the effective cavity volume and total magnetic moment (since the counterpart of  $J$  is proportional to the total magnetic moment, the resulting magnon-photon coupling strength becomes proportional to the square root of the total magnetic moment). Note that  $g_c$  gives the resonance field splitting. The frequency splitting, which represents the real magnon-magnon coupling strength, requires field-to-frequency conversion along the magnon dispersion curve. Because of the effective demagnetization field in the Kittel equation, the conversion factor is usually larger than the single-electron gyromagnetic ratio of 2.8 MHz/Oe.

The interfacial exchange coupling strength is determined by the electronic and lattice properties of the materials. Reported coupling strengths are  $J = 0.4$  mJ/m<sup>2</sup> for YIG/Co [30], and  $0.06$  mJ/m<sup>2</sup> for YIG/Py [33]. It is worth noting that as a back-to-back published paper with Ref. [30], a different mechanism, i.e. the dipole-dipole coupling of spin waves in YIG/Ni nanograting system, can also yield a similar interfacial magnon-magnon cou-

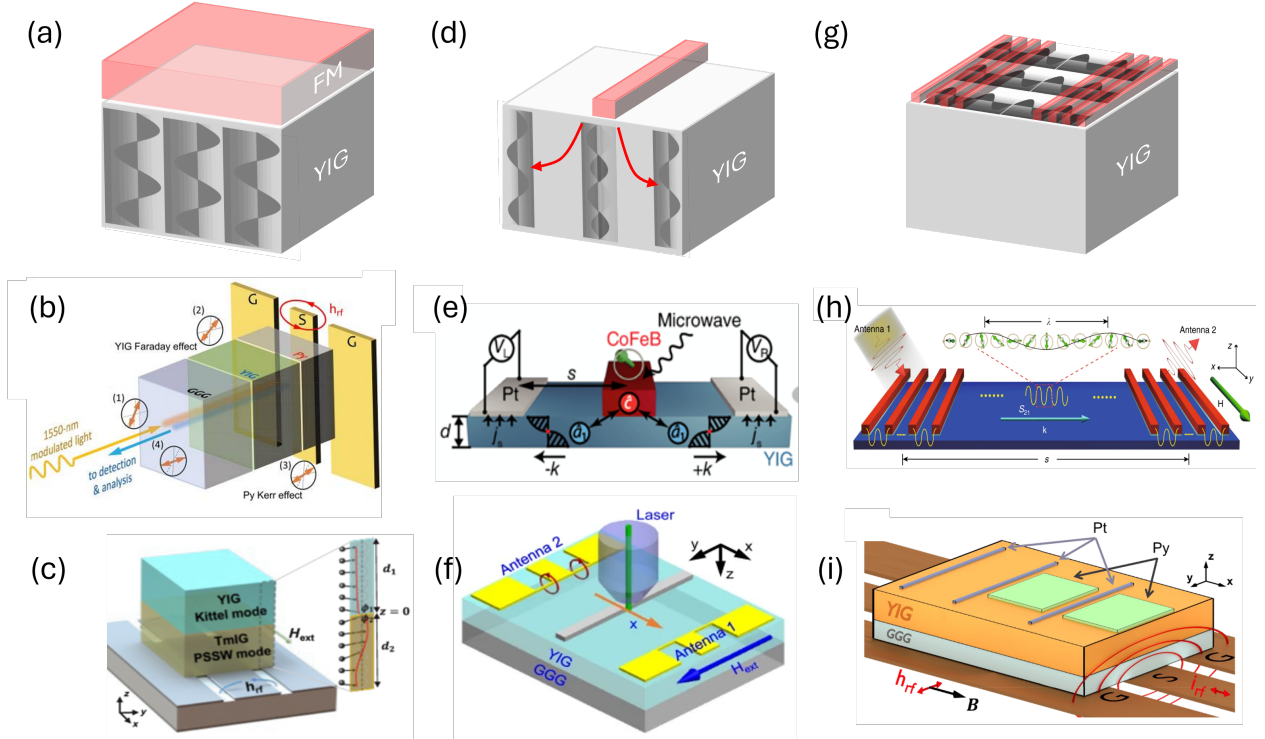


FIG. 4. The various geometries of magnon-magnon coupling in bilayer magnetic heterostructures. (a,b,c): uniform, extended bilayer coupling in which the thickness of the film defines the magnonic cavity, for (b) insulator/metal (Figure taken from Ref.[15]), and (c) all-insulator systems (Figure taken from Ref. [35]). (d,e,f): the device geometry in which an FM stripe couples locally to an extended YIG film. The excited magnons can propagate along the lateral dimension, and be detected via: (e) dc rectifications, e.g., using spin Hall effect of Pt (Figure taken from Ref. [93]), or (f) with rf inductive antennas and magneto-optical probes (Figure taken from Ref. [94]). (g,h,i): lateral magnonic cavity in which the FM stripes (h) serve as complementary, local antennas (Figure taken from Ref. [95]), or (i) only used to define the cavity boundaries while the excitation is globally sourced otherwise (Figure taken from Ref. [96]).

pling strength of  $0.03 \text{ mJ/m}^2$  [31]. The YIG/CoFeB interface exhibits a magnon-magnon anticrossing gap [32] similar to YIG/Py, suggesting that their  $J$  values are of the same order of magnitude. It is noted that the interfacial exchange coupling strength is significantly smaller than the intrinsic exchange coupling in ferromagnets. For example, in permalloy (Ni<sub>80</sub>Fe<sub>20</sub>, or Py) the interfacial exchange energy can be expressed as  $2A_{ex}/a$  where  $A_{ex}$  is the exchange constant and  $a$  is the lattice parameter [99]. Taking  $A_{ex} = 12 \text{ pJ/m}$  and  $a = 0.36 \text{ nm}$  for Py [92], one finds  $2A_{ex}/a = 68 \text{ mJ/m}^2$  which is 3 orders of magnitude larger than  $J$ .

The interfacial exchange coupling between YIG and metallic FM is found to be antiferromagnetic (i.e.,  $J$  is negative) in most bilayer systems, using magnetometry and neutron scattering [29, 30, 33, 100]. This is due to the oxygen-mediated superexchange coupling mechanism between the Fe-O bond in YIG and the metallic atoms (Fe or Co) in the adjacent FM layer [101, 102]. Nevertheless, a clean interfacial superexchange coupling would require careful processing of the surface, such as ion milling [33, 102] or acidic treatments, which has been shown to improve the interfacial spin pumping efficiency

[103]. Such AFM coupling has been deployed for several magnon manipulation strategies: e.g., Fan *et al.* [29] demonstrated a magnon spin valve by exploiting antiparallel magnetization configurations to suppress magnon transmission. Chen *et al.* [31] reported an enhanced magnon-magnon coupling in antiparallel (AP) Co/YIG bilayers compared to parallel (P) states.

In addition to the real part of the coupling ( $J$ ), an imaginary component ( $J'$ ) arises from spin pumping [33], an effect which describes the flow of pure spin current [104] between the two layers. This effect manifests as mutual damping enhancement (or reduction), depending on the symmetry of the hybrid magnon-magnon mode: the total linewidth increases for the out-of-phase hybrid mode and decreases for the in-phase mode in YIG/Py. In YIG/Py,  $J'$  is measured to be  $0.019 \pm 0.009 \text{ mJ/m}^2$ , which is about one third of  $J$ . This imaginary interfacial coupling works similarly as the dissipative coupling in cavity magnonics [105]. However, since it usually comes with the much stronger real interfacial exchange coupling, the observed magnon-magnon coupling is dominated by the level repulsion (avoided crossing) rather than level attraction.

*c. All-insulator system* To mitigate high dissipation in metallic films, recent works have expanded to all-insulator heterostructures. In such systems, both layers can exhibit significantly lower magnetic damping than metallic FM films, resulting in a higher cooperativity. In addition, the interface quality is also greatly enhanced due to epitaxy growth. For example, Liu *et al.* [35] achieved low-dissipation magnon-magnon coupling in epitaxial YIG/Tm<sub>3</sub>Fe<sub>5</sub>O<sub>12</sub>(TmIG) bilayers, where interfacial exchange coupling enables coherent interactions at practical frequencies and wavevectors, overcoming the limitations of YIG/Py systems. The YIG/TmIG system exhibits antiferromagnetic interfacial exchange coupling, similar to YIG/metallic FM systems, with a coupling strength of  $J \sim 0.06$  mJ/m<sup>2</sup>. Similarly, Li *et al.* [34] demonstrated programmable magnonic crystals in epitaxial YIG/Gd<sub>3</sub>Fe<sub>5</sub>O<sub>12</sub>(GdIG) by leveraging temperature-dependent Gd<sup>3+</sup> moments to switch between AFM and FM coupling, at the magnetization compensation temperature of GdIG around 200 K. The coupling strength is  $J \sim 0.5$  mJ/m<sup>2</sup> above 200 K, but it abruptly switches to  $-0.5$  mJ/m<sup>2</sup> below 200 K and further increases from  $-0.5$  mJ/m<sup>2</sup> to  $-1.7$  mJ/m<sup>2</sup> as the temperature decreased to 50 K. These advances highlight ferrimagnetic insulators as versatile platforms for quantum magnonics.

### Weakly-coupled sublattices in antiferromagnets

Antiferromagnets (AFMs) consist of spin sublattices with antiparallel alignment that fully compensate the total magnetization in the materials. Like other multilayer ferromagnets, the spin dynamics in AFMs exhibit acoustic modes and optical modes, which corresponds to the in-phase and out-of-phase dynamics of different spin sublattices. Nevertheless, because of the antiparallel spin alignment, the eigenfrequencies of the acoustic and optic modes formed by different spin sublattices evolve differently with an external magnetic field, leading to a reduction of the higher-frequency optical mode and an increase of the lower-frequency acoustic mode and, therefore, their mode intersection at a certain field. Under certain conditions which break the symmetry and lift the orthogonality of the acoustic and optical modes such as rotating the biasing field to off-axis directions, the two modes will couple to each other, yielding their mode anticrossing or magnon-magnon mode hybridization.

The recent discovery of 2D AFM families adds additional versatility to studying GHz-range AFM magnon-magnon coupling, because of the weak interlayer exchange coupling strength. Symmetry analysis of different AFM magnon modes is demonstrated to be an easy and effective method to predict if certain couplings exist or vanish, and thus can guide further experimental design. With the development of THz spectroscopy and ultra-fast laser technology, rich nonlinear effects have been uncovered in bulk AFM materials,

enabling exotic magnon mode operations including frequency up/down-conversion and second-harmonic generation. In the following section, we introduce the physical mechanisms and experimental results on the exchange-coupled magnons in AFM and 2D systems.

*d. 2D AFM* The advent of 2D AFM materials has opened new avenues for studying magnon coupling in atomically thin systems. MacNeill *et al.* [37] and Cham *et al.* [38] employed FMR to probe magnon interactions in CrCl<sub>3</sub> and CrSBr, respectively [Fig.5 (a-e)]. While both materials share a Hamiltonian with in-plane FM and interlayer AFM couplings, their anisotropy profiles differ dramatically: CrCl<sub>3</sub> exhibits negligible in-plane anisotropy, favoring spin-flop states under any in-plane field, whereas CrSBr's strong uniaxial anisotropy stabilizes antiparallel spin alignment below a critical field. For CrCl<sub>3</sub>, breaking the two-fold rotational symmetry of the coupled LLG equations around the in-plane field direction via an out-of-plane magnetic field component activates coupling between acoustic and optical magnon modes. In contrast, the same two-fold rotational symmetry around the in-plane easy axis of CrSBr can be broken by rotating the field in plane, creating an avoided crossing for acoustic and optical modes. Cham *et al.* [38] further observed chirality-selective coupling between left-handed (LH) and right-handed (RH) magnons, with triaxial anisotropy inducing a zero-field avoided crossing—a hallmark of strong mode hybridization. Most recently, Li *et al.* [40] reported ultrastrong coupling (normalized coupling rate  $\eta_{\text{eff}} = g_{\text{eff}}/(2\pi f_r) = 0.31$  exceeding 0.1) in CrPS<sub>4</sub>, attributed to magnetocrystalline anisotropy rather than exchange enhancement, alongside chirality-switchable sublattice magnons—a feature also tied to the orthorhombic anisotropy. In parallel, Cham *et al.* [106] recently demonstrated electrically tunable antiferromagnetic resonance in bilayer 2D AFMs using a spin-filter tunneling geometry, achieving both local detection and electrical control of magnon modes via spin-orbit torque-mediated damping modulation. This represents a major step toward integrating high-frequency AFM dynamics into nanoscale devices and leveraging sublattice-specific spin control for on-chip applications.

Despite these advances, significant challenges remains in probing 2D or bulk AFM magnon modes due to relatively weak FMR signals and their extension into the THz-frequency regime. These properties limit the effectiveness of conventional microwave techniques operating in the GHz range, which typically rely on magnetic susceptibility coupling. To address this, innovative optical approaches have emerged. For instance, Bae *et al.*, [107] developed an exciton-mediated pump-probe reflectivity method to detect magnon dynamics in 2D AFM CrSBr, where coherent magnon dynamics is directly observed. In this scheme, spectral shifts of exciton resonances act as a sensitive probe for spin precession, effectively serving as a magnon proxy [Fig.5 (f-j)]. The exciton resonance couples strongly to interlayer spin alignment, functioning as both a readout mechanism and a stabilizer for long-lived

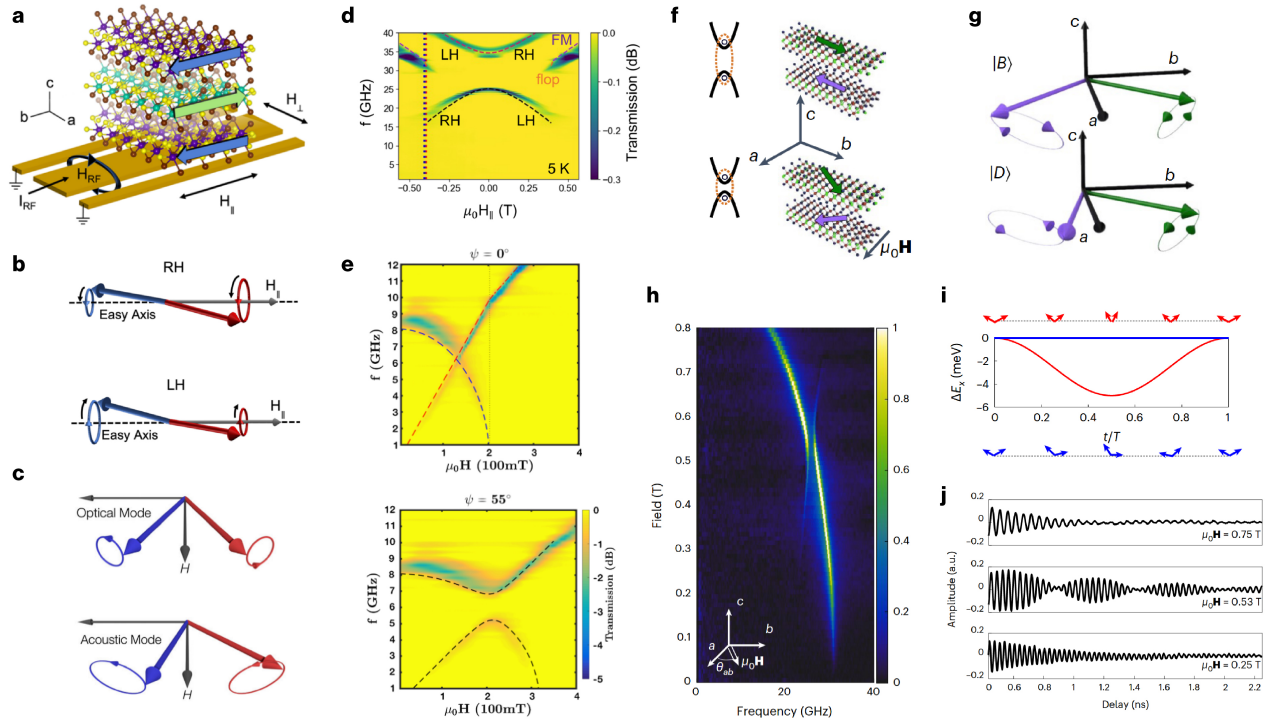


FIG. 5. Detecting magnon-magnon coupling in 2D AFM systems. (a) Schematic of microwave absorption experiment with 2D material. (b) Right-handed (RH) and left-handed (LH) magnon modes. (c) Optical and acoustic magnon modes. (d) Strong magnon-magnon coupling between RH and LH modes in CrSBr. (e) Strong magnon-magnon coupling between optical and acoustic modes in CrCl<sub>3</sub>. The coupling is only activated by breaking in-plane rotational symmetry. (f) Magnetic state alters the exciton resonance energy in CrSBr. (g) Bright and dark magnon modes. (h) Magnon dispersion detected with optical reflectivity measurements in CrSBr. (i) Calculated transient exciton resonance energy shift from the optical (red) and acoustic (blue) magnon modes. (j) Coherent magnon hybridization between bright and dark magnon modes detected by time-resolved measurement. (Figures (a-d) taken from Ref. [38]; (e) taken from Ref. [37]; (f-j) taken from Ref. [39].)

magnon modes. By tuning external magnetic fields and mechanical strain, precise control of opto-mechanical-magnonic coupling has been achieved [39]. With the improvement in measurement sensitivity, future study may uncover the unique layer-dependent magnon dynamics in 2D AFM systems.

*e. Bulk AFM* Using time-domain two-dimensional THz spectroscopy, Zhang *et al.* [42, 43] investigated the 3D canted antiferromagnets ErFeO<sub>3</sub> and YFeO<sub>3</sub> [Fig.6 (a,g-j)]. Under weak perturbations, both materials exhibit two magnon modes: the quasi-ferromagnetic (qFM) mode, corresponding to a precession of the magnetization orientation, and the quasi-antiferromagnetic (qAFM) mode, representing a periodic modulation of the magnetization amplitude [Fig.6 (e)]. Crucially, both ErFeO<sub>3</sub> and YFeO<sub>3</sub> possess Dzyaloshinskii-Moriya interactions that lead to canted magnetic moments. These canted moments break time-reversal symmetry and enable magnetic dipole-based nonlinear interactions [108]. By applying two-dimensional time-resolved THz spectroscopy, Zhang *et al.* were able to selectively and directly probe various types of coherent nonlinear magnon-magnon interactions in YFeO<sub>3</sub> [Fig.6 (f)]. Although the linear magnon response dominates in conventional one-

dimensional THz spectroscopy, the 2D technique revealed clear signatures of anharmonic magnon interactions in off-diagonal peaks, which arise from coherent interactions between the qAFM and qFM modes. Notably, second-order magnon processes—such as sum-frequency generation, second-harmonic generation, and difference-frequency generation—were observed for the first time [Fig.6 (j)]. Using a similar approach, the authors also demonstrated asymmetric up-conversion processes in ErFeO<sub>3</sub> [Fig.6 (g)]. It is important to emphasize that while strong THz-field driving is essential, the presence of two coupled resonant magnon modes (magnon-magnon coupling) is equally critical for enabling these asymmetric up-conversion processes.

### Syn-AFMs (RKKY-driven)

The RKKY interaction, a fundamental phenomenon in magnetism, plays a pivotal role in a variety of magnonic and spintronic applications. The RKKY interaction arises from the indirect coupling of spins in magnetic materials via conduction electrons. In this section, we summarize recent progress that has been made in understand-

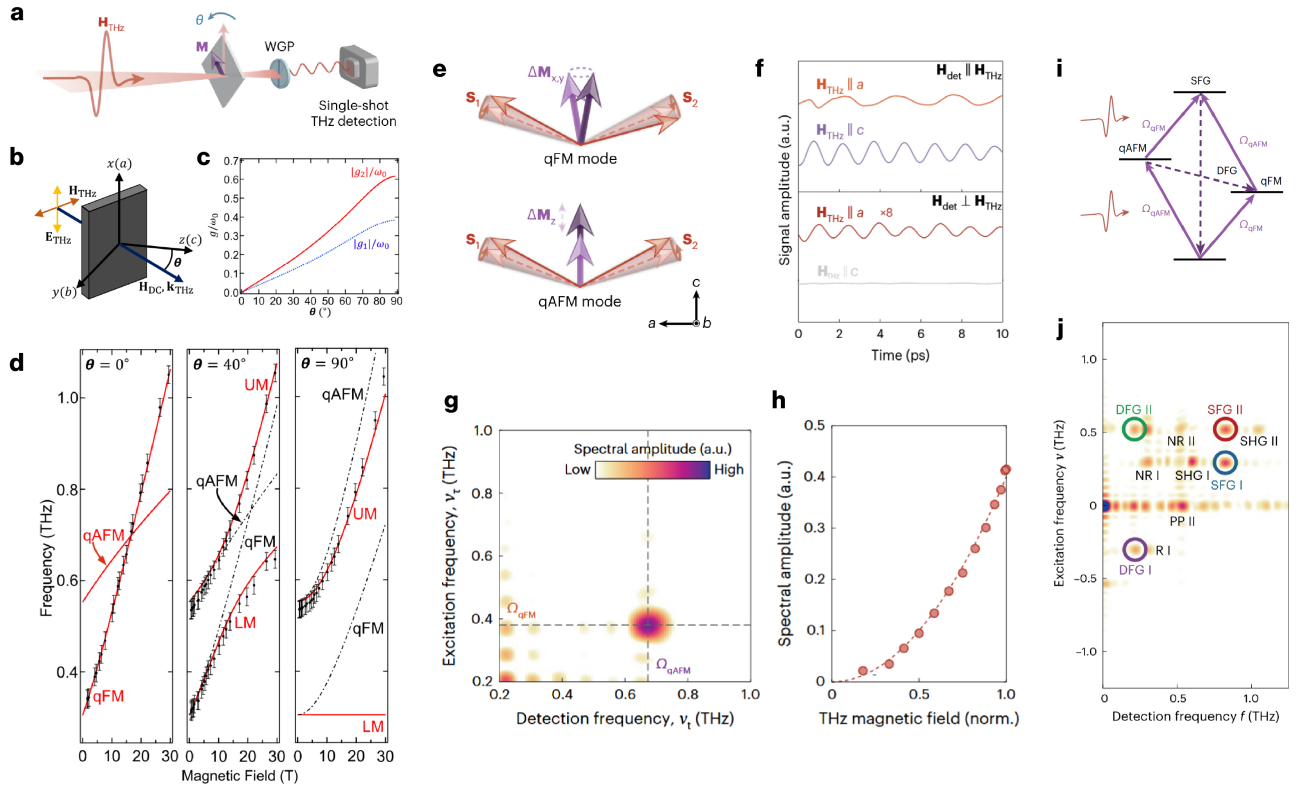


FIG. 6. Detecting magnon-magnon coupling in bulk AFM systems. (a) Schematic of time-resolved THz free induction decay (FID) measurement. (b) Sample geometry of  $\text{YFeO}_3$  in a tilted magnetic field to study the THz frequency magnon bands. (c) Calculated co-rotating (blue) and counter-rotating (red) coupling strengths show the dominance of the counter-rotating coupling terms. (d) Measured THz magnon bands and the ultra-strong magnon-magnon coupling in  $\text{YFeO}_3$ . (e) quasi-FM (qFM) and quasi-AFM (qAFM) magnon mode. (f) Excitation of different magnon modes in  $\text{ErFeO}_3$ . (g) Strong magnon frequency up-conversion illustrated in 2D THz FID spectra. (h) Dependence of the magnon up-conversion signal amplitude on the pump magnetic field. (i) Magnon energy-level diagrams. (j) The 2D THz spectra in  $\text{YFeO}_3$  summarizing the rich linear and nonlinear processes including pump-probe (PP), rephasing or photon echo (R), non-rephasing (NR), two-quantum (2Q), second harmonic generation (SHG), sum-frequency generation (SFG) and difference frequency generation (DFG). (Figures (a),(e),(i),(j) taken from Ref. [43]; (b-d) taken from Ref. [41]; (f-h) taken from Ref. [42].)

ing the nature of magnon-magnon interactions within magnetic heterostructures which utilize the RKKY interaction.

*f. Metallic multilayer syn-AFMs* In multilayer heterostructures, comprised of magnetic thin films separated by nonmagnetic spacer layers, the magnetic films can be exchange coupled by the RKKY interaction. The best known structure in this category is the syn-AFMs. A conventional syn-AFM structure consists of two magnetic thin films separated/coupled together via one spacer layer. Often, the only anisotropy within the magnetic layers is from the shape of the magnetic layers, e.g., many syn-AFMs behave like easy-plane antiferromagnets. In an easy-plane antiferromagnet, there are two antiferromagnetic resonance (AFMR,  $k = 0$ ) magnon modes that can be excited with a uniform driving field. The so-called acoustic AFMR mode has a zero frequency at zero field, and increases linearly with the applied external field. The so-called optical AFMR mode has a finite frequency at zero field, which is proportional to the square root of the

product of the interlayer exchange field and the magnetization of the individual layers. The frequency of the optical AFMR mode decreases as the external magnetic field increases. At some finite external field, these two modes will encounter energy degeneracy, and there will be a crossing point. The magnon-magnon interactions that are studied in these RKKY coupled materials most often tend to hybridize the acoustic and optical AFMR modes in the vicinity of this crossing point. Consequently, these interactions manifest as an avoided energy level crossing between the two modes of interest.

Before delving into the origins of the magnon-magnon interactions in syn-AFMs, it is important to first describe the role that the RKKY interaction plays in dictating the general dynamic properties of a syn-AFM. Importantly, the strength of the interlayer RKKY exchange interaction greatly impacts the external field and frequency where the acoustic and optical magnon modes cross. So, although the RKKY interaction is not necessarily responsible for the magnon-magnon interaction within a syn-

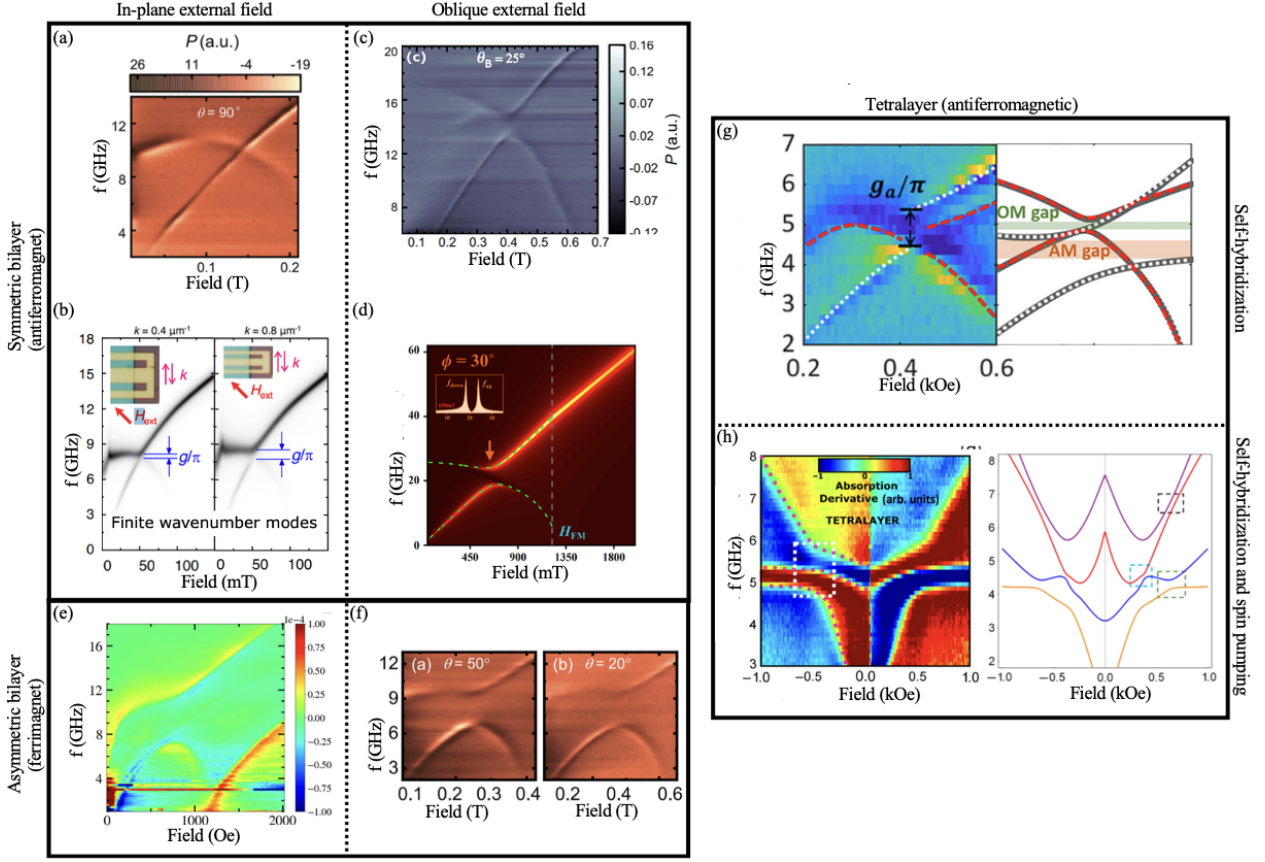


FIG. 7. Interactions between acoustic and optical magnons in synthetic magnets are summarized above. The upper left portion of the figure illustrates how, for synthetic antiferromagnets, the crossing between an acoustic and optical branch [(a)] can turn into an avoided crossing by changing the wave number [(b)], or applying a symmetry breaking external field oblique to the sample plane, [(c), (d)]. The respective references for these images are taken from [109], [110], [111], and [112]. Similar avoided crossings are shown in the lower left portion of the figure in a synthetic ferrimagnet, where the magnetic layers have unequal thicknesses or dissimilar magnetizations, [(e), (f)] taken from Ref. [109, 113]. An alternative strategy to engineer interactions into these materials is by changing the number of magnetic layers. The right portion of the figure, [(g), (h)] taken from Ref. [62, 114], shows how in a tetralayer, acoustic or optical magnon pairs interact. If interlayer spin pumping is present in the tetralayer, optical and acoustic magnon pairs can interact as well without the aid of a symmetry breaking field.

AFM, it is responsible for the presence of both optical and acoustic modes as well as the field-frequency pairs where the modes interact. Therefore, if one is motivated to investigate magnon-magnon interactions at higher frequencies, it is important to optimize the strength of the RKKY interaction itself. In recent years, the most commonly used spacer layer is ruthenium. Many of the highest zero-field optical magnon frequencies, above 20 GHz, have been reported in CoFeB/Ru systems [115–117]. More recently, in syn-AFM structures comprised of Co and Ru, the antiferromagnetic interlayer exchange interaction was further enhanced by alloying the Ru spacer layer with magnetic materials, e.g., Co and Fe [118].

*g. Magnonic Interactions in syn-AFMs* Following the report of tunable magnon-magnon interaction in layered  $\text{CrCl}_3$  crystals in 2019 [37], the same tunable interaction was demonstrated by Sud *et al.*, in an syn-AFM with easy-plane anisotropy [111]. This interaction, between the uniform ( $k = 0$ ) acoustic and optical magnon modes,

is controlled by tilting the external field out of the easy plane, as shown in Fig. 7(c) and (d). The origin of this interaction is from the external field breaking the two-fold rotational symmetry of the system, as explained for 2D AFM materials, which in general exists in any easy-plane antiferromagnet [37, 111, 112, 119]. This symmetry can also be broken by intrinsic aspects of a syn-AFM. He *et al.* demonstrated that weak uniaxial anisotropy could be induced in systems like CoFeB/Ir/CoFeB. In this system, the magnon mode gap could be tuned based on the orientation of the external field relative to the easy and hard axes [120]. Similarly, Wang *et al.* theoretically and experimentally explored how asymmetric magnetic anisotropies of the two ferromagnetic layers in a FM/NM/FM structured syn-AFM can be used in lieu of the out-of-plane field to hybridize the uniform acoustic and optical magnon mode [56].

An alternative way to hybridize acoustic and optical magnons in easy-plane syn-AFM was demonstrated by

Shiota *et al.* [110], [Fig. 7 (b)]. Their work showed that by adjusting the in-plane magnetic field direction relative to the wave vector of the excited magnon modes, they could modulate the coupling strength, with stronger coupling observed at higher wave numbers. In these experiments, no out-of-plane external field was required; the magnon-magnon interaction originated from dynamic dipolar fields generated between the layers when the wave number was non-zero.

It is also possible to engineer magnon-magnon interactions into syn-AFMs, without the aid of symmetry breaking external fields, through the use of layer number-dependent effects. For example, by altering the structure of a syn-AFM to have four layers the AFMR spectra are altered to have two optical and two acoustic modes. The pairs of all-optical, or all-acoustic modes “self-hybridize” with each other without the aid of a symmetry breaking external field [72]. This self-hybridization manifests as characteristic avoided energy level crossing between the acoustic or optical pair of modes. Micromagnetic simulations have been used to demonstrate the potential for electrically tuning this type of magnon-magnon interaction within a tetralayer [72]. Rong *et al.* recently demonstrated these effects, and observed how the presence or absence of magnon-magnon interactions was strongly dependent on the number of layers in syn-AFMs [114]. In particular, they observed magnon-magnon interactions arising from self-hybridization within the even-layered syn-AFMs, as shown in Fig. 7(g), while odd-layered syn-AFMs exhibited avoided energy level crossings due to the structural asymmetry within the syn-AFM. In similar tetralayer structures, Subedi *et al.* also observed an avoided energy level crossing between optical and acoustic magnons, as shown in Fig. 7(h), which could not be attributed to the self-hybridization effect. Here, the magnon-magnon interaction arises from symmetry breaking which in this case is amplified by interlayer dynamic field-like torques originated through spin pumping between the interior and surface layers of the structures [62]. When small structural asymmetries (interfacial roughness) exist within a syn-AFM, the additional dynamic field-like torques, from spin pumping, generate a symmetry breaking field that is strong enough to clearly hybridize acoustic and optical magnons.

*h. Magnonic Interactions in synthetic Ferro- and Ferri-magnets* In addition to synthetic antiferromagnets, one can create both synthetic ferrimagnets and ferromagnets. A synthetic ferrimagnet can be made by modifying a conventional synthetic antiferromagnet such that the net magnetic moment in each magnetic layer (or sub-lattice) is different. For example, ferrimagnetic behavior can be observed in structures where magnetic layers have unequal thicknesses, dissimilar ferromagnetic materials, or an odd number of magnetic layers [52, 53, 109, 113]. Magnon-magnon interactions in synthetic ferrimagnets, where the magnetic layers have different thicknesses and/or the magnetic layers are comprised of different magnetic materials, have been explored

[109, 113], as shown in Fig.7(e) and (f). In the case of a synthetic ferrimagnet, with two magnetic layers, there is an optical and acoustic ferrimagnetic resonance mode akin to the modes found in a syn-AFM. In a synthetic ferrimagnet, these modes naturally hybridize since the coupled LLG equations are intrinsically not symmetric under the symmetry operation where the magnetization of each layer is rotated around the external field by 180° and then followed by a layer swap.

In RKKY coupled systems, synthetic ferromagnets are materials where the magnetic thin films are separated by a spacer layer which promotes a ferromagnetic interlayer exchange coupling. In these materials, it is generally more difficult to characterize the strength of the RKKY interaction and to excite any magnon mode aside from the uniform (acoustic) mode. In general, characterization of the RKKY interaction is difficult due to the tendency for the two layers to be aligned. Magnetometry cannot be used to estimate the interlayer exchange interaction between two magnetic thin films unless the magnetization is non-collinear. The excitation of optical magnon modes in a synthetic ferromagnet is difficult because it requires a spatially non-uniform driving field. Conventional FMR-based techniques typically generate spatially uniform fields that can only couple to the acoustic mode, which behaves like a conventional Kittel-like mode even in the presence of the interlayer coupling. These challenges, perhaps, underpin the relative lack of experimental progress in studying magnon-magnon interactions with synthetic ferromagnetic materials.

Another class of synthetic magnets, with magnonic properties that have not been well explored experimentally, is comprised of magnetic layers with orthogonal anisotropies or tilted anisotropies. Such structures have been theoretically modeled using the Landau Lifshitz equations [121] as well as micromagnetic simulations [122]. In the case of two magnetic layers with orthogonal anisotropies, the coupling between acoustic and optical magnon modes was investigated as both a function of the interlayer exchange interaction as well as the saturation magnetization. In the case of two magnetic layers with tilted anisotropy, the interplay of *both* the external field tilt and the anisotropy tilt on the interaction strength between the acoustic and optical magnon modes were investigated. Synthetic magnets with orthogonal anisotropies are also a promising material platform because they have recently been shown to house interlayer antisymmetric exchange interactions that oscillate as a function of the spacer layer thickness, which strongly indicates an RKKY origin [123].

## Dipolar coupling

The generation, manipulation, and detection of spin waves at the nanoscale are three key research directions in Magnonics. Recently, a significant mechanism for spin-wave manipulation at nanoscale has emerged—dynamic

dipolar coupling, which complements static dipolar coupling.

Dynamic dipolar coupling occurs when oscillating magnetic moments in one material (e.g., a  $\text{Ni}_{81}\text{Fe}_{19}$  ferromagnetic stripe) or one element in an array generate time-varying magnetic fields that interact with moments in another material (e.g., YIG) or another element of the array. This interaction alters the spin-wave dispersion relation by modifying the effective magnetic field. The static dipolar field induced by the first material or element shifts the entire spin-wave dispersion in the second material or element, while the dynamic dipolar field created by the first element induces changes within a narrow frequency range near resonance in the second layer. This offers additional functionality including magnon-magnon coupling and hybridization [126–131]. This coupling is strongest when materials are in close proximity, separated only by a thin nonmagnetic spacer, and is highly dependent on their relative magnetization orientations.

One key effect of dynamic dipolar coupling is the downshift of the spin-wave dispersion relation in a continuous YIG film caused by dynamic dipolar coupling to a ferromagnetic metal nanostripe [124], enabling mode conversion and nanoscale control. For instance, time-resolved magneto-optical Kerr effect (TR-MOKE) microscopy in a YIG/CoFeB bilayer shows that this coupling induces a frequency downshift, reducing spin-wave wavelengths from  $12.8\ \mu\text{m}$  to  $310\ \text{nm}$  at  $1.76\ \text{GHz}$  [124] [Fig. 8(a) and (b)]. Similarly, Talapatra *et al.* observed wavelength reductions from  $3.4\text{--}7.5\ \mu\text{m}$  to  $280\text{--}480\ \text{nm}$  at the YIG/Co interface, as seen in time-resolved scanning transmission x-ray microscopy (TR-STXM) images [125] [Fig. 8(c)].

Beyond dispersion control, dynamic dipolar coupling facilitates reconfigurable spin-wave transport. It has been used in hybrid YIG-based material structures that function as Fabry-Pérot nano-resonators [124], where overlapping spin waves interfere constructively (in-phase) or destructively (out-of-phase), analogous to optical interference. The resonance condition in these structures depends on path length, wavelength, and phase shifts at interfaces or boundaries. Complementing these studies, Santos *et al.* demonstrated an order-of-magnitude increase in magnon confinement in a YIG film region not covered by the ferromagnetic metal, preserving YIG’s optimal magnetic properties within the cavity [132]. Furthermore, the fabrication of micrometer-sized YIG cavities—created between two YIG/Permalloy bilayers—in an on-chip formulation offers a novel approach for coherent magnon control where a nanometer-sized Pt strip has been shown to function as a noninvasive local detector of magnon resonance intensity via spin pumping [132].

Nonreciprocity—where spin-wave propagation differs depending on direction—enhances magnonic functionality. Qin *et al.* achieved partial and full nonreciprocity in YIG hybrid structures, with narrow FM stripes ( $730\ \text{nm}$  width) exhibiting asymmetric dispersion and wider FM stripes ( $>25\ \mu\text{m}$  width) showing damping-related differences, respectively [124].

Chiral scattering of spin waves, driven by dynamic dipolar coupling, has also been investigated. Fripp *et al.* used micromagnetic simulations and a phenomenological model to explore this effect in a ferromagnetic thin film coupled to a nanoscale magnonic resonator [133]. They demonstrated strong, nonreciprocal scattering, where the resonator’s precession induces direction-dependent effects via quasi-uniform (13.5 GHz) and dark (17.4 GHz) modes. This coupling, termed chiral due to its handedness in relation to spin-wave momentum, enables the development of magnonic diodes and phase shifters, offering promising avenues for scalable spin-wave control.

Recent studies have extended the exploration of dynamic dipolar coupling to artificial spin lattices. A notable example is a dipolarly coupled trilayer system composed of  $\text{Ni}_{81}\text{Fe}_{19}$  (30 nm)/Al (35 nm)/ $\text{Ni}_{81}\text{Fe}_{19}$  (20 nm) nanobars arranged in a square lattice [126, 134]. The thicker nanobars were found to switch at higher fields compared to the 20 nm  $\text{Ni}_{81}\text{Fe}_{19}$  layers. Spin-wave spectroscopy revealed a nominal 1 GHz frequency shift between configurations where the top and bottom layers were anti-aligned versus aligned [126] [Fig. 8(d)]. Additionally, the application of external magnetic fields at different in-plane angles resulted in further reconfiguration of the spin-wave spectra [134].

Another type of dynamically coupled systems emerges if artificial-ice lattices patterned on the top of continuous thin film underlayers. Negrello *et al.* showed that an array of stadium-shaped NiFe nanoislands deposited on the top of a continuous NiFe film with non-magnetic spacer layers of varying thickness results in distinct modes in the film at either specific wavelengths or with intensity modulation imprinted by the artificial spin-ice system [131]. This type of dynamic mode coupling in the vertical direction, facilitated by dipolar coupling, enables the modulation of spin-wave propagation at nanometer length scales [130, 131].

Besides in magnetic multilayers, the dynamic dipolar coupling can also arise in arrays of magnetic micro- and nanostructures if the constituent elements of the array are sufficiently close to one another [128, 129, 135–138]. For example, strong magnon-magnon coupling was observed in crossshaped nanoring arrays, nanocross arrays, and artificial spin ice systems. Interestingly, Adhikari and co-workers observed an enhancement of inter-element-dynamic dipolar interactions leading to avoided level-crossing and nonlinear frequency shifts [137].

The next step in this direction can involve integrating 3D nanostructures onto on-chip resonators and employing both global spin pumping and local probe techniques, such as Brillouin light scattering microscopy [Fig. 8(e)]. The in-plane dipolar and exchange coupling can be further tuned by modifying disconnected and interconnected networks of nanobars on periodic and aperiodic [139] lattices. Additionally, a systematic reduction in periodicity through controlled disorder [140] could provide new avenues for engineering magnonic behavior.

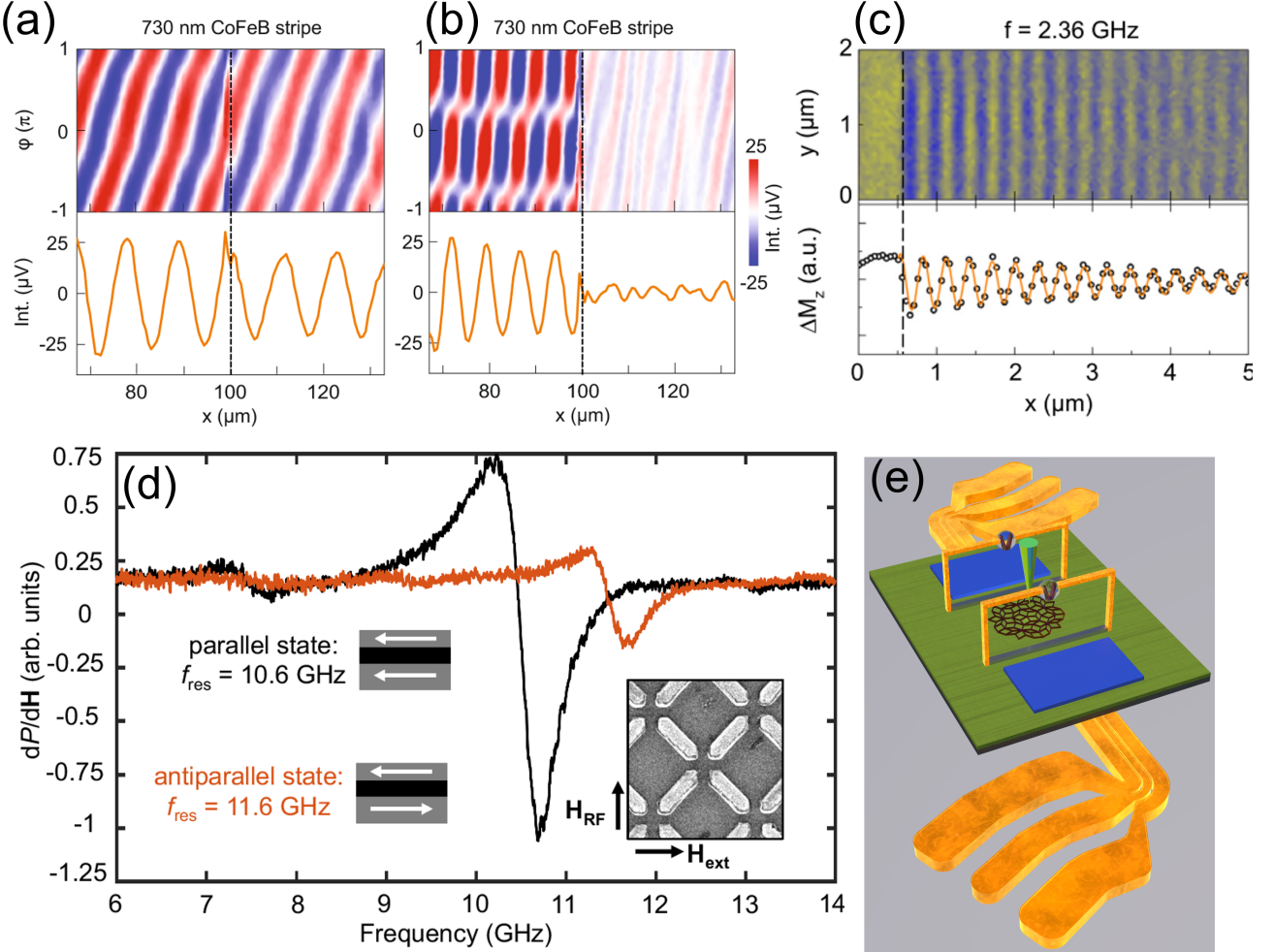


FIG. 8. (a), (b) Phase-resolved TR-MOKE microscopy maps and line profiles measured on a 100-nm-thick  $\text{Y}_3\text{Fe}_5\text{O}_{12}$  (YIG) film with a 730-nm-wide CoFeB stripe. Figure taken from ref. [124]. (c) High-resolution normalized TR-STXM images and line profiles of propagating short-wavelength spin waves in the YIG/Co bilayer at 2.36 GHz with a 10 mT bias field. Figure taken from ref. [125]. (d) Ferromagnetic resonance (FMR) spectra for parallel (black) and antiparallel (red) macrospin states, showing a 1 GHz frequency shift between the states at  $H_{\text{ext}} = 0$ . An SEM schematic defines the DC external field  $H_{\text{ext}}$  and RF field  $H_{\text{RF}}$  orientations for the FMR data panels in this figure. Figure taken from ref. [126]. (e) Schematic of the proposed all-on-chip device inspired by previous studies on dynamic dipolar coupling. The  $\text{Ni}_{81}\text{Fe}_{19}$  (blue), Penrose P3 nanomagnet arrays (maroon), and Pt (gray) are patterned on plain YIG (dark green). The entire chip is placed on an RF co-planar waveguide (CPW). A global spin-pumping voltage can be determined by connecting a nanovoltmeter to the Pt stripes, whereas the local mode profile can be obtained using BLS methods (bright green indicating the laser).

These advancements in dynamic dipolar coupling, non-reciprocity, and artificial spin lattices pave the way for scalable, reconfigurable magnonic devices with applications in wave-based computing, signal processing, and nanoscale information transport [141, 142].

#### Dzyaloshinskii–Moriya interaction (DMI)

The DMI favors an orthogonal spin configuration. It can be described using a Hamiltonian given by,  $\mathbf{H}_{\text{DM}} = -\mathbf{D}_{12} \cdot (\mathbf{S}_1 \times \mathbf{S}_2)$ , where  $\mathbf{D}_{12}$  is the DMI vector,  $\mathbf{S}_1$  and  $\mathbf{S}_2$  are two atomic spins. The competition between the DMI and other types of spin-spin interactions,

such as the Heisenberg exchange interaction, which favors a collinear spin configuration, enables the stabilization of a diverse range of unconventional spin textures (e.g., skyrmions). The presence of a large DMI simultaneously requires a broken inversion symmetry and strong spin-orbit coupling (SOC) in the framework of the three-site model proposed by Fert and Levy [147, 148]. The breaking of inversion symmetry can occur naturally in lattices of crystals [149], such as B20 metals (e.g.,  $\text{Fe}_{1-x}\text{Co}_x\text{Si}$  [150],  $\text{FeGe}$  [151],  $\text{MnSi}$  [152]) and insulators with similar crystal structure (e.g.,  $\text{Cu}_2\text{OSeO}_3$  [153]), leading to the so-called bulk DMI. Broken inversion symmetry can also exist at the interfaces of magnetic thin films and multilayers [154], leading to the in-

Systems	freq. (GHz)	Coupl. strength (GHz)	Magnon modes	Coupl. types	Ref.
<b>Direct-Ex (Magnet-1 / Magnet-2)</b>					
YIG(100 nm)/NiFe(9 nm)	–	0.35	PSSW/FMR	SC	[33]
YIG(3000 nm)/NiFe(10 nm)	4-8	0.09	PSSW/FMR	MIT	[15, 16]
YIG(3000 nm)/NiFe(30 nm)	2.5-3.5	0.022	PSSW/FMR	MIT/SSC	[18]
YIG(100 nm)/NiFe(30 nm)	1-9	–	BVSW/MSSW	MIT	[96]
YIG(20 nm)/Co(30 nm)	–	0.79	PSSW/FMR	SC/USC	[31]
YIG(20 nm)/Ni(20 nm)	–	0.12	PSSW/FMR	SC/USC	[31]
YIG(1000 nm)/Co(50 nm)	0-25	0.2	PSSW/FMR	SC	[30]
YIG(295 nm)/CoFeB(50 nm)	2-8	–	PSSW/FMR	SC	[32]
TmIG(350 nm)/CoFeB(50 nm)	–	0.263	PSSW/FMR	SC	[35]
TmIG(140 nm)/YIG(140 nm)	–	0.105	PSSW/FMR	SC	[35]
GdIG(74 nm)/YIG(46 nm)	10-15	0.5(150 K)	PSSW/FMR	SC	[34]
<b>Direct-Ex (AFM Magnet)</b>					
CrCl <sub>3</sub> (crystal)	10-25	0-1.37(1.56 K)	Acoustic/Optic	SC	[37]
CrSBr (crystal)	15-40	4(100 K)	Acoustic/Optic	SC/Chiral	[38]
CrSBr (flake, 20 nm)	20-30	~ 8(35 K)	Acoustic/Optic	SC/Strain	[39]
CrPS <sub>4</sub> (crystal)	10-25	>4(22.5 K)	Acoustic/Optic	USC/Chiral	[40]
YFeO <sub>3</sub> (crystal)	~ 600-1000	>350	qAFM/qFM	USC	[41]
<b>Dipolar</b>					
YIG(70 nm)/CoFeB(stripe)	–	–	MSSW/BVSW	–	[94]
YIG(80 nm)/CoFeB(stripe)	1-13	–	PSSW	–	[93]
YIG(30 nm,PMA)/CoFeB(stripe)	5-10	–	FVSW	MIT	[143]
YIG(20 nm)/Co(grating)	15-20	0.62	MSSW/PSSW	MIT	[48, 95]
NiFe(44 nm, film)	10-15	~1	MSSW/PSSW	SC	[144]
NiFe(20 nm)/YIG(3900 nm)	10-15	0.5/1.3	MSSW/PSSW	SC	[145]
NiFe(20 nm, cross array)	–	–	MSSW	MIT	[135]
NiFe(30 nm, spin ice)	5-11	3.275	Acoustic/Optic	USC	[126]
<b>RKKY (Magnet / Interlayer)</b>					
CoFeB(15 nm)/Ru(0.6 nm)	3-17	0-0.67	Acoustic/Optic	SC	[110]
CoFeB(3 nm)/Ru(0.5 nm)	5-20	~1	Acoustic/Optic	SC	[111]
(Co/Ni)/Ir(0.6 nm)	0-18	>4	Acoustic/Optic	USC/DSC	[56]
NiFe(3.1 nm)/Ru(1 nm)	2-7	0.556	Acoustic/Optic	SC	[114]
NiFe(5 nm)/Ru(1 nm)	2-8	–	Acoustic/Optic	SC	[146]
<b>DMI</b>					
(CH <sub>3</sub> CH <sub>2</sub> NH <sub>3</sub> ) <sub>2</sub> CuCl <sub>4</sub>	2-5	>0.27(2.5 K)	Acoustic/Optic	SC	[54]

TABLE I. Summary of the current magnon-magnon material systems exhibiting different coupling frequencies, coupling strengths, involved magnon modes, and coupling types. Involved magnon modes – PSSW: perpendicular standing spin wave; FMR: ferromagnetic resonance (Kittel mode); MSSW: magnetostatic spin wave; FVSW: forward volume spin wave; BVSW: backward volume spin wave; Acoustic(optic): in-phase(out-of-phase) coupled resonances in syn-AFMs; qAFM(qFM): AFM(FM)-coupled spin resonances in crystal AFM. Coupling types – SC: strong coupling, defined as the coupling strength  $g$  being greater than the dissipation rates of both magnon counterparts,  $g > \gamma_{m1}, \gamma_{m2}$ ; MIT: magnetically-induced transparency, defined as the coupling strength being greater than the dissipation of one mode but less than the other,  $\gamma_{m1} > g > \gamma_{m2}$ ; USC, ultrastrong coupling, defined as the coupling strength  $g$  being comparable to (a fraction of) the bare mode frequencies of the uncoupled systems; DSC, deep strong coupling: defined as the coupling strength  $g$  being greater than the bare mode frequencies of the uncoupled systems; SSC: superstrong coupling, defined as the coupling strength  $g$  being comparable to the free-spectral range (FSR).

terfacial DMI where the coupling between two atomic spins ( $\mathbf{S}_1$  and  $\mathbf{S}_2$ ) in a thin magnetic layer is mediated by a third atom with strong SOC in a neighboring non-magnetic or magnetic layer. This opens up potential for tailoring the interfacial DMI by materials design (heterostructure, strain, chemical doping), which has been demonstrated in ferromagnet/heavy-metal [154], antiferromagnet/heavy-metal [155–157], and recently, insulating magnets based system (Pt/TmIG/GGG [158] and substrate/rare-earth(RE)IG/metal trilayer [159]), and synthetic antiferromagnets [160, 161] where two atomic spins from two neighboring ferromagnetic lay-

ers can even have DMI through the large-SOC atoms in the paramagnetic spacers [160]. Such interlayer-type interfacial DMI is thus different from the conventional intralayer-type interfacial DMI where the two atomic spins reside in the same magnetic layer.

The manifestation of DMI in magnon-magnon coupled system has remained scarce and been limited to synthetic antiferromagnet (syn-AFM) based systems [162, 163], where the ultrastrong magnon-magnon coupling is predicted by tailoring the interplay among the magnetic anisotropy field, the effective interlayer DMI field, and the effective RKKY interaction field [163]. At present,

it remains unclear how the synergistic interaction among DMI, direct exchange interaction, and RKKY interaction at the interface of two magnetically ordered layers influences the magnon-magnon coupling. To address this fundamental question, it is imperative to develop low-damping magnetic heterostructures with tunable spin-spin interactions of different types (DMI, direct exchange, and RKKY). One approach is to insert a composite interface layer [164] such as  $\text{Fe}_{1-x}\text{Pt}_x$  between the Py and YIG.

*A multi-coupling scheme* Magnon-magnon coupling in the presence of a combined, synergistically-controlled interfacial coupling scheme is a particularly interesting material engineering direction for hybrid magnonics. For example, combining analytical theory and magneto-optical measurement, a recent work [25] has demonstrated the capability of exploiting the synergistic effect of Zeeman torque and exchange torque at a Py/YIG interface to tune the spin precessional phase of the PSSW mode in the YIG, hence opening new potential application as phase-controlled hybrid magnonics. Looking ahead, using the above-mentioned Py/ $\text{Fe}_{1-x}\text{Pt}_x$ /YIG heterostructure as an example, *how to understand, predict, and characterize the synergistic effect of interfacial DMI and direct exchange coupling on the phase, amplitude, and wavevector-dependence of the magnons in the YIG?*

From a theoretical/computational perspective, addressing this question requires a new analytical or micromagnetic model that can predict the magnetic susceptibility and coupled magnon-magnon dynamics in a multiphase system with coexistence of interfacial exchange coupling and interfacial DMI at the interface of two dissimilar magnetic layers, and can be further coupled to photon and/or acoustic phonon subsystems. To this end, the first step would be to develop a generalized magnetic boundary condition that simultaneously allows a partial transfer of exchange torque, the magnetic energy flow conservation across the interface, and the minimization of the magnetic interface energy (which is contributed by both the isotropic exchange energy and the anisotropic DMI energy[165]).

To date, existing theories and computational models only permit a rigorous treatment of the boundary conditions associated with the direct exchange coupling between two magnetic layers (e.g., the Hoffman boundary condition [166, 167]), the interfacial DMI between a magnetic layer and a non-magnetic layer [168, 169], and more recently, the interlayer DMI in a Syn-AFM [170]. Although a generalized Barnas-Mills boundary condition has been developed for a finite-thickness interface with the coexistence of DMI and direct exchange interaction [171], such a boundary condition has not yet been implemented in any analytical and numerical studies related to magnon-magnon coupling or evaluated in comprehension.

## FUTURE PERSPECTIVE OF MAGNON-MAGNON HYBRID MATERIALS SYSTEM

The discovery of magnon-magnon coupling in various material systems offers a new approach to modulating and controlling intrinsic magnon excitations, potentially enabling new applications in coherent magnon engineering across a wide range of hybrid magnonic platforms. Below we highlight several representative hybrid magnonic systems that incorporate magnon-magnon hybrid materials, and explore how magnon-magnon coupling can enhance and expand the capabilities of magnon-based coherent information processing, summarized in Fig. 9.

### Magnon-photon interaction

*Strong coupling and magnon-magnon gap* Magnon-photon coupling is the fundamental interaction in cavity magnonics, originating from the strong magnetic dipolar coupling between magnetic excitations and electromagnetic waves. Through cavity-enhanced interaction, strong magnon-photon coupling can be achieved, enabling coherent energy transduction between magnons and microwave photons [174–176]. This mechanism forms the foundation of quantum magnonics [2], where magnon-qubit entanglement can be realized, mediated by cavity microwave photon acting as a coherent data bus.

By incorporating magnetic materials with magnon-magnon coupling, one can modulate the efficiency of magnon-photon coupling via the magnon-magnon bandgap. An example is the layered hybrid perovskite antiferromagnet  $(\text{CH}_3\text{CH}_2\text{NH}_3)_2\text{CuCl}_4$  (Cu-EA) [54]. In Cu-EA, the intrinsic interlayer coupling features antiferromagnetic type. In addition, the structure-induced DMI breaks the symmetry, and hence leads to the hybridization of interlayer acoustic and optical magnon modes, manifesting a magnon-magnon bandgap at their crossing point. In addition, the position of this magnon bandgap can be sensitively tuned by temperature as a result of changes in the interlayer antiferromagnetic coupling strength. When the frequency of a resonator mode lies within the magnon-magnon bandgap, the magnon excitations become decoupled from the microwave photons, effectively disabling the magnon-photon interaction. This effect was demonstrated by Li *et al.* [172], where a Cu-EA crystal was coupled to a coplanar superconducting resonator in a flip-chip configuration. As the temperature varies, the magnon-photon anticrossing gap closed and reopened as the magnon-magnon band gap shifted across the resonator frequency. Consequently, the magnon-photon coupling strength varied from 35 MHz at 1.5 K, dropped to zero between 3 and 3.5 K, and then increased to 42 MHz at 6 K. In particular, the temperature range of zero coupling can be engineered by designing the resonator frequency to coincide with the desired location

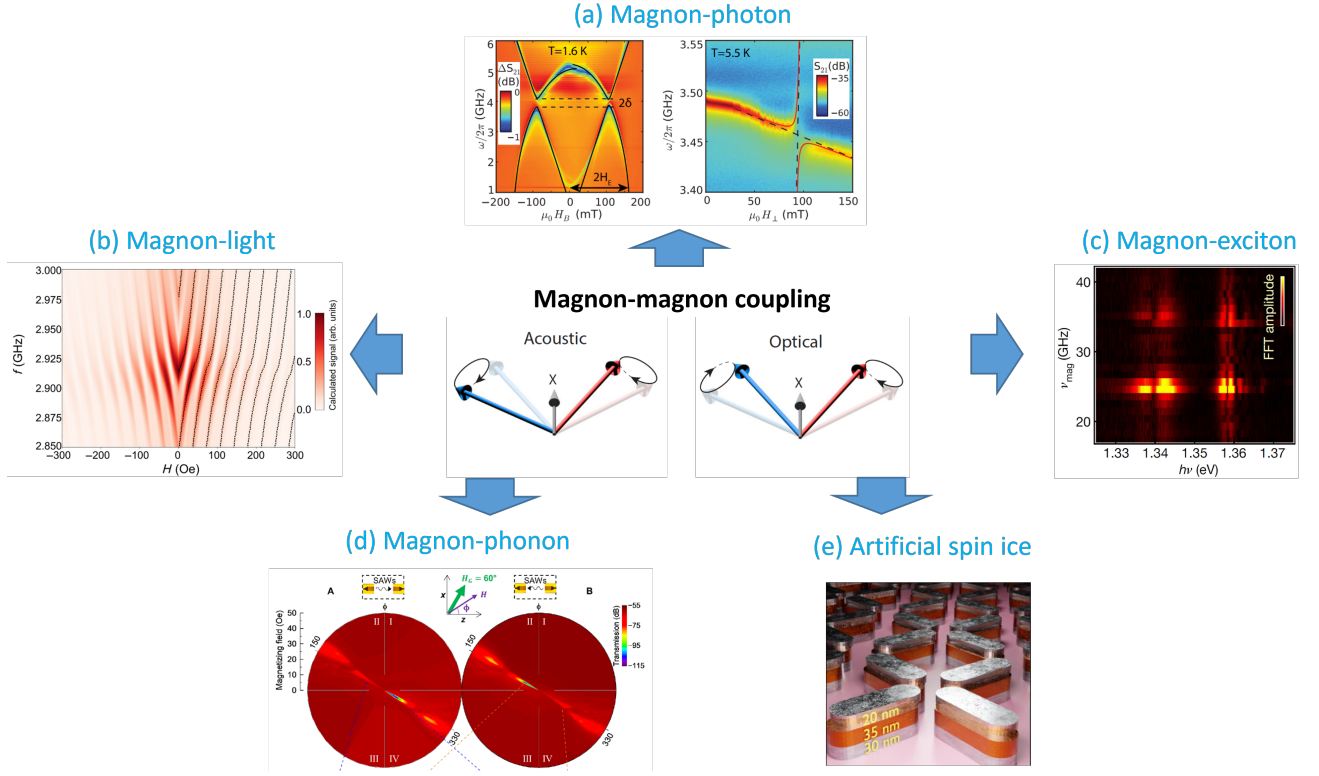


FIG. 9. Future perspective of magnon-magnon coupling as an approach to modulate interactions in other hybrid magnonic systems. Examples including (top to bottom): (a) tuning magnon-photon interaction via magnon-magnon gap, figure taken from Ref. [172]; (b) modulating magnon-light interaction and spectrum using magneto-optical effect and its inverse, figure taken from Ref. [18]; (c) synergy with magnon-exciton modulation, figure taken from Ref. [107]; (d) nonreciprocal magnon-phonon interaction due to magnon-magnon coupling, figure taken from Ref. [173]; (e) artificial spin ice system leveraging magnon-magnon coupling, figure taken from Ref. [126].

within the magnon-magnon bandgap.

The demonstration highlights the opportunity to manipulate coherent mode hybridization and control coherent information processing with quantum properties in complex magnetic materials. Another similar example is to use a superconducting resonator to investigate magnon-magnon coupling between two remote quasi-two-dimensional topological magnets Cu[1,3-benzenedicarboxylate(bdc)] via their mutual magnon-photon coupling to the resonator [177]. In addition, the use of cavity magnonics also provides a new way to probe complex spin-wave dispersion with narrow-band microwave characterizations instead of broad-band ferromagnetic resonance. Similar ideas can also be implemented with other magnon-magnon hybrid materials with different magnon bandgap engineering.

*Purcell regime and superstrong coupling* Another example is when the magnon-magnon coupling is in the intermediate regime, in which one magnon mode simply enhances or attenuates the excitation of the other magnon counterpart, e.g. the cavity modes in the confined geometry. In this case, as introduced earlier, a magnonic cavity can be formed [18]. The excited cavity modes can then interact with additional photon mode in a multi-partite

coupling scheme. In the earlier example by Inman *et al.*, a photon resonator mode is provided by a split-ring resonator, which couples to a magnon-magnon coupled YIG/Py bilayer. The Kittel mode of YIG couples to the photon mode directly, forming a strong coupling anti-crossing. In addition, the cavity modes of YIG (prompted by the Py) can also couple to the photon mode, exhibiting a superstrong coupling spectrum, i.e. when the coupling strength is of the same order of the free-spectral range (FSR) [178], and in the present example, the FSR can be neatly tuned by the cavity size (thickness of YIG).

### Magnon-light interaction

Optical light, known for its low-loss propagation, resilience to environmental noise and high bandwidth, is the backbone of modern communication systems and shows strong potential for the next-generation information processing and transduction such as photonic integrated circuits [179], quantum optics [180] and quantum communication [5]. While electro-optic [181] and optomechanical [182] systems are the main-stream approaches for converting optical information to solid-state signals,

magneto-optical systems have emerged as promising alternatives due to their broad frequency tunability and unique nonreciprocity for implementing on-chip photonic isolators [183–185]. Magnon-light interactions can occur through magneto-optical coupling such as the Faraday effects in bulk materials and Kerr effect at the interface, where the light polarization is modified by the magnetic moment and thus modulated by the magnetic excitations [186, 187]. This process has been demonstrated using YIG sphere resonators via interactions between the Kittel magnon mode and whispering-gallery optical modes [188, 189]. Recent advances target on-chip optomagnonic resonators based on single-crystalline YIG thin films [190, 191], which offer enhanced mode overlap and reduced volume, enabling stronger and more efficient magnon-optical interactions.

The introduction of magnon-magnon hybrid material system can highly enrich magnon-light modulation. By depositing a metallic ferromagnetic thin film, such as Py, on one side of a YIG film, the Py layer acts as a mirror which can reflect optical light that is normal incident from the other side of the YIG film. This YIG/Py bilayer acts as a magneto-optical modulator where both the Faraday effect in YIG and the Kerr effect at YIG/Py interface contribute to the light polarization rotation [15–17, 25, 192]. Note that due to the sign reversal of both the light chirality and wavevector during reflection, the Faraday effect of the reflected light in YIG contributes with the same sign as the incident light, doubling the Faraday signal. The coherent coupling between YIG and Py changes the symmetry of the YIG PSSW modes with short wavelengths, allowing them to couple with external uniform microwave field. This has led to a series of new coherent phenomena in magneto-optical interactions, such as magnetically-induced transparency [11, 15, 16] and zero-reflection [24, 25]. Specifically, the magnon-magnon coupling can:

- (i) allow to leverage the various interfacial coupling types with distinct symmetries (direct-exchange, RKKY, and DMI) to operate in a single or collective fashion, so as to fully exploit the rich spin wave dispersions (beyond just Kittel magnon mode). This can be realized via engineering the film(or nanostructure)'s size and dimension, excitation geometry, and magnetic field.
- (ii) make the overall concept of using film-based structures more compatible with the state-of-the-art photonic and phononic architectures, and can thus be seamlessly integrated in an all-on-chip format. In particular, the magnonic waveguide resonators can be further subject to additional electrical, optical, or mechanical control knobs (the available CMOS toolkit) [75, 94, 193–195].
- (iii) provide a platform for accessing and controlling magnon-light transduction exploiting unconventional magnon modes or collective states, such as the magnon BEC mode, in the presence of strong nonlinear magnon processes, such as three- and four-magnon scatterings [22].

## Magnon-phonon interaction

The coupling between magnons and acoustic phonons represents the dynamical energy exchange between the spin and lattice subsystem of a material. Similarly to other hybrid magnonic systems, the coupling strength represents the rate of the energy exchange, which is proportional to the magnetoelastic coupling constant and the mode profile overlap [196–198]. Since magnetoelastic coupling coefficient is a fourth-order tensor, this interaction energy density is essentially nonzero in any materials that have a nonzero net magnetization in the entire body (ferro-/ferri-magnets) or its sublattice (ferri-/antiferro-magnets). This universality provides flexibility in the selection of materials platform for studying magnetoelastic interactions. Additionally, the frequency and wavenumber of the magnons and acoustic phonons for most magnetically ordered materials are not too distinct in the GHz-THz range, making it efficient to either excite magnons by acoustic phonons [199–211] and vice versa. For example, by leveraging the developments from the field of microelectromechanical systems, such as the surface acoustic wave (SAW) or bulk acoustic wave (BAW) based devices, and the field of picosecond ultrasonics [212], efficient acoustic excitation of magnons has been demonstrated experimentally at both the GHz and THz regime. Due to such flexibility in materials and device design, hybrid magnon-phonon system has emerged as one of the most intensively studied hybrid magnonic systems, which has been utilized to realize coherent gate operation for quantum information science applications [6, 207], enable long-distance (mm-scale) magnon transport [200], and design dynamically tunable, narrowband THz emitters [197, 208, 209] and THz optoelectronic transducer [211] (see detailed discussion of device architectures in relevant patents [213–216]).

The combination of magnon-magnon coupling with magnon-phonon coupling has enabled emergent functionalities, such as the nonreciprocal transmission of SAWs in a hybrid system comprised of a FeGaB/Al<sub>2</sub>O<sub>3</sub>/FeGaB multilayer integrated onto a LiNbO<sub>3</sub>-based SAW device [173]. Specifically, the magnetic dipolar coupling between the two FeGaB layers gives rise to asymmetric magnon dispersion relation with respect to positive and negative wavevectors. As a result, for a fixed frequency, the resonant magnon-phonon interaction, where the frequencies and wavenumbers of both the magnons and acoustic phonons are identical, only occurs when the wavevector is, for example, negative. This would then lead to strong absorption of an SAW (i.e., its energy is transferred to the magnetic subsystem) that has a negative wavevector, whereas the SAW with a positive wavevector can transmit with much lower level of absorption. In a similar spirit, we expect that the magnon-magnon coupling, especially the synergistic interaction of different types of spin-spin coupling (direct exchange, DMI, RKKY, etc.), can further enrich the magnon-phonon coupling by introducing new features in the magnon dis-

persion relation and hence its overlap with the acoustic phonon dispersion. We suggest that recently developed TmIG/YIG multilayer [217] and rare-earth iron garnet superlattice such as TbIG/TmIG [218] are promising material candidates for studying such interplay between magnon-magnon coupling and magnon-phonon coupling for three reasons. First, the possible coexistence of direct exchange and DMI at the garnet/garnet interface enables the study of such a competing spin-spin interaction on magnon-phonon coupling. Second, epitaxial strain can be used to tune the orientation of ground-state magnetization in such iron garnet thin films, such as the introduction of perpendicular magnetic anisotropy[218–220] or noncollinear magnetization configuration, thereby enabling new functionalities into both magnon-magnon coupling (see [221] for a recent example) and magnon-phonon coupling. Third, it is possible to simultaneously engineer the magnon and phonon dispersion relation by superlattice design via band folding.

### Magnon-exciton interaction

An exciton is a bound state of a pair of electron and hole which are coupled via direct Coulomb interaction in a solid. In two-dimensional semiconductors, many show strong exciton excitations due to the significantly reduced dielectric screening of Coulomb interaction. These excitons couple strongly to light and persist to room temperature, allowing rich features in physics to be explored optically. In addition to exciton-light coupling, excitons can also couple to magnons due to spin-dependent electron and hole transfer, with the recent example of 2D magnetic semiconductor CrSBr [107]. This novel optical approach of probing magnon-electron interaction has been widely utilized to investigate polariton-magnon coupling [222], propagating magnons [107, 223], strain effects [224] and magnetic-field-controlled magnon-magnon hybridization [225], as well as higher-harmonic generation [226]. The degree of magnon-exciton hopping is determined by the spatial and spinor components of the exciton wavefunction overlap between layers. Since the structure is fixed, the spatial wavefunction overlap is fixed and the spinor part can be tuned using an external magnetic field [227]. Among various 2D magnetic semiconductors, this coupling is only observed in CrSBr because of its highly dispersive electronic band structure, leading to Wannier-type, delocalized excitons [107]. For instance, the magnetic semiconductor NiPS<sub>3</sub> and the magnetic insulator CrI<sub>3</sub> exhibit spatially localized, Frenkel-type excitons, and do not possess the similar spin-dependent charge transfer[228–230].

The introduction of magnon-magnon coupling in CrSBr, due to its nature of layered van der Waals antiferromagnet [38], brings a new approach to modulate magnon-exciton coupling by controlling the symmetry of the magnon-magnon hybrid modes. Recently, Diederich *et al.* [225] demonstrated that coexisting

magnon-magnon and magnon-exciton couplings can turn a dark acoustic magnon mode into a bright mode. Without magnon-magnon coupling, only the optical mode is bright because the optical mode involves changes in canting angle, whereas the acoustic mode has a fixed canting angle. However, applying an external field breaks the two-fold rotational symmetry and creates a hybridized mode between acoustic and optical magnons [38]. When the two modes are hybridized, both become bright and can be easily detected using the exciton sensing method. The coexisting magnon-magnon and magnon-exciton couplings in CrSBr also allow efficient generation and detection of nonlinear magnon dynamics such as magnon high-harmonic generation, parametric amplification, and sum- and difference-frequency generation [226].

Besides magnon-exciton coupling, another feature of CrSBr is its strong magnetoelastic coupling [231]. Compared to three-dimensional magnets, two-dimensional magnetic systems often display enhanced magnetoelastic interactions due to the confinement of spin interactions within the in-plane direction [232]. How these multiple coexisting couplings interact to give rise to new magnonic phenomena remains an open and intriguing area of research.

### Floquet engineering of hybrid magnonic systems

Floquet engineering, the application of a time-periodic external field, has become an efficient method to control electronic and spintronic properties and create new coherent states in quantum materials [89]. In hybrid magnonic systems, Floquet engineering has thus far been implemented via the application of either a continuous sinusoidal magnetic field or periodic pulses. Several new functionalities such as Floquet-induced magnonic Autler-Townes splitting [233] and on-demand dark-bright mode conversion [234] have been experimentally demonstrated in hybrid magnon-photon systems based on bulk YIG spheres. Furthermore, Floquet control of magnonic Rabi oscillation (where the Rabi flopping frequency between two magnon polariton modes was tuned by varying the amplitude of continuous Floquet drive) and magnonic Ramsey interference (where the relative phase difference between the two modes was controlled by frequency detuning and the control of free evolution time under pulsed Floquet drive) have been computationally demonstrated in practical-sized 3D hybrid magnon-phonon cavity based on YIG spheres [4]. Looking ahead, driven by the need of miniaturization, power reduction, and on-chip heterogeneous integration, we envisage opportunities and challenges rising in (i) the extension of Floquet Engineering to on-chip hybrid magnonic systems (especially the magnon-phonon cavity), and (ii) the adoption of Floquet fields that are easier to localize on a chip such as r.f. voltage-induced surface acoustic waves and current-induced spin torques.

Beyond device-level control, Floquet engineering enables access to intrinsically nonequilibrium phenomena with no equilibrium analogue. One prominent example is the creation of a synthetic frequency (time) dimension, in which harmonics of a driven mode constitute a lattice and the Berry curvature defined over momentum–frequency (Sambe) space governs topological energy transfer between tones—a generalized Thouless pump in frequency space [235]. Although explored in photonics and other quantum platforms, this framework carries over naturally to cavity magnonics, where strong coherent magnon–photon coupling and periodic control of coupling and detuning have been demonstrated [236], and the interplay between coherent and dissipative couplings under Floquet driving has been analyzed in detail theoretically [237]. A complementary opportunity is offered by leveraging the interplay of periodic drive and dissipation to realize non-Hermitian Floquet phases, including PT-symmetric and PT-broken regimes characterized by exceptional points, mode coalescence, non-orthogonal eigenmodes, and enhanced susceptibility [238]. This perspective has recently been translated to microwave cavity platforms, where tailoring the time dependence of dissipation in tandem with Floquet modulation implements a non-Hermitian shortcut to adiabaticity, enabling fast, high-fidelity state transfer [239]. Although this exploration is only beginning—particularly on the experimental front—the convergence of Floquet control, hybrid magnonics, and engineered dissipation clearly signals substantial potential for realizing and harnessing nonequilibrium phases and functionalities beyond equilibrium platforms.

### Computing with artificial spin ice

Artificial spin ice (ASI) [58, 240–243] systems are increasingly recognized as promising physical platforms for neuromorphic computing owing to their vast microstate landscapes, intrinsic non-linear dynamics, and reconfigurability [139, 140, 244–249]. ASI consists of lithographically fabricated 2D arrays of nanomagnets arranged in periodic or aperiodic lattices, offering a versatile platform to study magnetic states absent in natural materials. Initially conceived as mesoscopic analogs of frustrated pyrochlores [250, 251], ASI has since evolved into a rich field of its own.

Typically, each nanomagnet acts like a binary Ising-like macrospin by selecting the aspect ratio of individual nanomagnets in these lattice to ensure a single-domain state [58]. However, for certain applications, a bistable macrospin–vortex configuration in individual nanomagnets can be advantageous [126, 247]. The collective behavior at lattice vertices enables direct access to frustration, emergent monopole–antimonopole excitations, and phase transitions. These systems also hold promise as reprogrammable magnonic crystals, where spin waves function as coherent information carriers [252–255].

Moreover, the collective interactions within these nanomagnet arrays naturally support paradigms like reservoir computing, processing temporal information efficiently by harnessing internal dynamics [247, 256]. Extending these systems into three dimensions (3D), especially via vertically stacked layers, significantly enhances their potential [126, 257, 258]. Recent work demonstrates that purely dipolar coupling between layers can achieve ultrastrong magnon–magnon interaction without direct exchange, enabling highly tunable magnonic metamaterials that overcome traditional coupling-reconfigurability trade-offs [126, 259]. This 3D approach allows for substantial zero-field mode shifts, the generation of distinct hybrid modes (acoustic/optical), and phase control, offering unprecedented spectral manipulation for future devices and enhanced neuromorphic capabilities through richer dynamics and exponentially larger state spaces (e.g.,  $16^N$  vs  $2^N$ ) [126, 247–249].

Looking ahead, the refined control offered by 3D ASI opens avenues beyond conventional neuromorphic computing into areas like spin logic and wave-based processing [260]. The ability to program distinct microstates, each with a unique magnonic spectral fingerprint, improves readout and computational power [129, 248]. Furthermore, functionalities like chirality-selective control of vortex states using inter-layer dipolar fields act as programmable switches, introducing spectral asymmetries useful for low-field sensing or information encoding [126]. Manipulating hybridized modes with specific phase relationships is also key for coherent magnonics, potentially enabling phase-based logic and directional information flow [260]. Future research will likely focus on integrating more layers or diverse materials (including antiferromagnets or active spacers, such as Ru, and 2D magnets) and further exploring these chiral and non-reciprocal effects within complex 3D structures to unlock new functionalities [261, 262].

## CONCLUSION

As a new subfield of hybrid magnonics, magnon–magnon coupling focuses on the fundamental interactions between magnon modes through material engineering. This includes interfacial exchange engineering in magnetic bilayers, magnon band structure engineering in van der Waals antiferromagnets or synthetic antiferromagnets, and dipolar field engineering in nanomagnet arrays. These magnetic interactions offer a means to control and design magnon eigenmodes, akin to electron band structure engineering but accessible via electrical excitation and detection at microwave frequencies. Moreover, since magnon–magnon coupling occurs within engineered magnetic materials, it can be seamlessly integrated with other hybrid magnonic systems, enabling the potential modulation of magnon– $X$  coupling through magnon band engineering.

As a summary of the section of future perspectives, we

anticipate three major directions for future developments in magnon-magnon coupling, as i) creating new functionalities for magnon-based coherent information processing and transduction in coupling to other dynamic systems, such as microwave photons, acoustic phonons, optical light, and excitons; ii) investigating fundamental physics in novel quantum materials, such as spin-electron (magnon-exciton) coupling in layered van der Waals antiferromagnets, and Dzyaloshinskii-Moriya interaction in hybrid organic perovskite antiferromagnets; iii) advancing spin-wave computation schemes using artificial nanomagnetic networks. In all three directions, we remark on the importance of identifying suitable materials or hybrid material systems with large magnon-magnon coupling strengths and low magnon dampings for achieving strong coupling or ultrastrong coupling. Promising examples of low-damping materials include YIG and TmIG (magnetic insulators), Py and CoFeB (metallic ferromagnets), CrCl<sub>3</sub> and CrSBr (layered van der Waals antiferromagnets). In dipolar- and exchange-governed systems, additional structural engineering, such as reducing the film thickness or decreasing the spacing between adjacent nanomagnets, can also boost the coupling strength. As a conclusion, magnon-magnon coupling is a rapidly growing field expanding in materials science, quantum engineering, and with high potential of developing into a dynamic interdisciplinary field in hybrid magnonics.

## ACKNOWLEDGMENTS

W.Z. and Y.X. acknowledge support from the National Science Foundation under Grant No. NSF DMR-2509513. J.-M.Hu acknowledges support from the National Science Foundation under Grant No. DMR-2237884 and partial support for manuscript preparation from the Wisconsin MRSEC (DMR-2309000). M.M.S

and J.S. acknowledge support from the National Science Foundation under DMR-2328787. M.B.J. acknowledges support from the National Science Foundation under Grant No. 2339475. V.S.B. was supported by the U.S. Department of Energy, Office of Science, Office of Basic Energy Sciences under Award Number DE-SC-0024346. L.L. and Q.W. acknowledge support from National Science Foundation under Grant No. ECCS-2309838. The effort from Y.L. in paper writing was support by the U.S. DOE, Office of Science, Basic Energy Sciences, Materials Sciences and Engineering Division under contract No. DE-SC0022060. B. F. acknowledges support from the National Science Foundation under Grant No. NSF DMR-2144086. Y.K.L. acknowledges support from U.S. Department of Energy, Office of Basic Energy Sciences (DE-SC0025422).

## COMPETING INTERESTS

W.Z., Y.X., J.-M.H., J.S., M.M.S., V.S.B., Y.L., L.L., Q.W., Y.K.L., Y.J.B., B.F. declare no financial or non-financial competing interests. M.B.J. serves as an Editor of this journal and had no role in the peer-review or decision to publish this manuscript. M.B.J. declares no financial competing interests.

## AUTHOR CONTRIBUTIONS

W.Z., Y.L., J.H., J.S., B.J. conceived the project and wrote the initial version of the manuscript. W.Z., Y.L. organized the figures and the table. All authors contributed to the writing and editing of the manuscript. All authors have read and approved the manuscript.

## REFERENCES

---

- [1] G. Kurizki, P. Bertet, Y. Kubo, K. Mølmer, D. Petrosyan, P. Rabl, and J. Schmiedmayer, Quantum technologies with hybrid systems, *Proceedings of the National Academy of Sciences* **112**, 3866 (2015).
- [2] D. Lachance-Quirion, Y. Tabuchi, A. Gloppe, K. Usami, and Y. Nakamura, Hybrid quantum systems based on magnonics, *Applied Physics Express* **12**, 070101 (2019).
- [3] M. Zhang, C. Wang, Y. Hu, A. Shams-Ansari, T. Ren, S. Fan, and M. Lončar, Electronically programmable photonic molecule, *Nature Photonics* **13**, 36 (2019).
- [4] S. Zhuang, Y. Zhu, C. Zhong, L. Jiang, X. Zhang, and J.-M. Hu, Dynamical phase-field model of cavity electromagnonic systems, *npj Computational Materials* **10**, 191 (2024).
- [5] D. Awschalom, K. K. Berggren, H. Bernien, S. Bhave, L. D. Carr, P. Davids, S. E. Economou, D. Englund, A. Faraon, M. Fejer, S. Guha, M. V. Gustafsson, E. Hu, L. Jiang, J. Kim, B. Korzh, P. Kumar, P. G. Kwiat, M. Lončar, M. D. Lukin, D. A. Miller, C. Monroe, S. W. Nam, P. Narang, J. S. Orcutt, M. G. Raymer, A. H. Safavi-Naeini, M. Spiropulu, K. Srinivasan, S. Sun, J. Vučović, E. Waks, R. Walsworth, A. M. Weiner, and Z. Zhang, Development of quantum interconnects (quics) for next-generation information technologies, *PRX Quantum* **2**, 017002 (2021).
- [6] Y. Li, W. Zhang, V. Tyberkevych, W.-K. Kwok, A. Hoffmann, and V. Novosad, Hybrid magnonics: Physics, circuits, and applications for coherent information processing, *Journal of Applied Physics* **128**, 130902 (2020).
- [7] H. Yuan, Y. Cao, A. Kamra, R. A. Duine, and P. Yan, Quantum magnonics: When magnon spintronics meets quantum information science, *Physics Reports* **965**, 1 (2022).
- [8] B. Flebus, D. Grundler, B. Rana, Y. Otani, I. Barsukov, A. Barman, G. Gubbiotti, P. Landeros, J. Akerman,

U. S. Ebels, *et al.*, The 2024 magnonics roadmap, *Journal of Physics: Condensed Matter* (2024).

[9] A. V. Chumak, P. Kabos, M. Wu, C. Abert, C. Adelmann, A. Adeyeye, J. Åkerman, F. G. Aliev, A. Anane, A. Awad, *et al.*, Advances in magnetics roadmap on spin-wave computing, *IEEE Transactions on Magnetics* **58**, 1 (2022).

[10] M. Goryachev, W. G. Farr, D. L. Creedon, Y. Fan, M. Kostylev, and M. E. Tobar, High-cooperativity cavity qed with magnons at microwave frequencies, *Physical Review Applied* **2**, 054002 (2014).

[11] X. Zhang, C.-L. Zou, L. Jiang, and H. X. Tang, Strongly coupled magnons and cavity microwave photons, *Physical review letters* **113**, 156401 (2014).

[12] Y. Tabuchi, S. Ishino, T. Ishikawa, R. Yamazaki, K. Usami, and Y. Nakamura, Hybridizing ferromagnetic magnons and microwave photons in the quantum limit, *Physical review letters* **113**, 083603 (2014).

[13] Y.-P. Wang and C.-M. Hu, Dissipative couplings in cavity magnonics, *Journal of Applied Physics* **127** (2020).

[14] M. Harder, Y. Yang, B. Yao, C. Yu, J. Rao, Y. Gui, R. Stamps, and C.-M. Hu, Level attraction due to dissipative magnon-photon coupling, *Physical review letters* **121**, 137203 (2018).

[15] Y. Xiong, Y. Li, M. Hammami, R. Bidthanapally, J. Sklenar, X. Zhang, H. Qu, G. Srinivasan, J. Pearson, A. Hoffmann, *et al.*, Probing magnon-magnon coupling in exchange coupled y 3 fe 5 o 12/permalloy bilayers with magneto-optical effects, *Scientific Reports* **10**, 12548 (2020).

[16] Y. Xiong, J. Inman, Z. Li, K. Xie, R. Bidthanapally, J. Sklenar, P. Li, S. Louis, V. Tyberkevych, H. Qu, *et al.*, Tunable magnetically induced transparency spectra in magnon-magnon coupled y 3 fe 5 o 12/permalloy bilayers, *Physical Review Applied* **17**, 044010 (2022).

[17] Y. Xiong, A. Christy, M. Mahdi, R. Sun, Y. Li, R. D. Geil, J. F. Cahoon, F. Tsui, B. Yang, T. H. Kim, *et al.*, Phase-resolving spin-wave microscopy using infrared strobe light, *Physical Review Applied* **22**, 064081 (2024).

[18] J. Inman, Y. Xiong, R. Bidthanapally, S. Louis, V. Tyberkevych, H. Qu, J. Sklenar, V. Novosad, Y. Li, X. Zhang, *et al.*, Hybrid magnonics for short-wavelength spin waves facilitated by a magnetic heterostructure, *Physical Review Applied* **17**, 044034 (2022).

[19] J. Rao, B. Yao, C. Wang, C. Zhang, T. Yu, and W. Lu, Unveiling a pump-induced magnon mode via its strong interaction with walker modes, *Physical Review Letters* **130**, 046705 (2023).

[20] F. Yang, C. Wang, Z. Chen, K. Zhao, W. Liu, S. Ma, C. Wei, J. Song, J. Rao, and B. Yao, Control of the coupled magnons with pumps, *Chinese Physics B* (2025).

[21] Y. Xiong, J. M. Nair, A. Christy, J. F. Cahoon, A. Pishehvar, X. Zhang, B. Flebus, and W. Zhang, Magnon-photon coupling in an opto-electro-magnonic oscillator, *npj Spintronics* **2**, 9 (2024).

[22] T. Qu, Y. Xiong, X. Zhang, Y. Li, and W. Zhang, Pump-induced magnon anticrossing due to three-magnon splitting and confluence, *Physical Review B* **111**, L180410 (2025).

[23] J. Wu, S. Zhou, B. Flebus, and W. Zhang, Coupling magnons to an opto-electronic parametric oscillator, *APL Photonics* **10** (2025).

[24] J. Qian, C. Meng, J. Rao, Z. Rao, Z. An, Y. Gui, and C.-M. Hu, Non-hermitian control between absorption and transparency in perfect zero-reflection magnonics, *Nature Communications* **14**, 3437 (2023).

[25] A. Christy, Y. Zhu, Y. Li, Y. Xiong, T. Qu, F. Tsui, J. F. Cahoon, B. Yang, J.-M. Hu, and W. Zhang, Tuning magneto-optical zero reflection via dual-channel hybrid magnonics, *Physical Review Applied* **24**, 034045 (2025).

[26] Y. Yang, Y.-P. Wang, J. Rao, Y. Gui, B. Yao, W. Lu, and C.-M. Hu, Unconventional singularity in anti-parity-time symmetric cavity magnonics, *Physical Review Letters* **125**, 147202 (2020).

[27] X. Zhang, K. Ding, X. Zhou, J. Xu, and D. Jin, Experimental observation of an exceptional surface in synthetic dimensions with magnon polaritons, *Physical review letters* **123**, 237202 (2019).

[28] Y. Xiong, A. Christy, Y. Li, R. Sun, A. H. Comstock, J. Wu, R. Lopez, S. Lei, D. Sun, J. F. Cahoon, *et al.*, Photon-magnon coupling using gain-assisted spoof-localized surface plasmons, *Optics Express* **33**, 16809 (2025).

[29] Y. Fan, P. Quarterman, J. Finley, J. Han, P. Zhang, J. T. Hou, M. D. Stiles, A. J. Grutter, and L. Liu, Manipulation of coupling and magnon transport in magnetic metal-insulator hybrid structures, *Physical Review Applied* **13**, 061002 (2020).

[30] S. Klingler, V. Amin, S. Geprägs, K. Ganzhorn, H. Maier-Flaig, M. Althammer, H. Huebl, R. Gross, R. D. McMichael, M. D. Stiles, *et al.*, Spin-torque excitation of perpendicular standing spin waves in coupled yig/co heterostructures, *Physical review letters* **120**, 127201 (2018).

[31] J. Chen, C. Liu, T. Liu, Y. Xiao, K. Xia, G. E. Bauer, M. Wu, and H. Yu, Strong interlayer magnon-magnon coupling in magnetic metal-insulator hybrid nanostructures, *Physical review letters* **120**, 217202 (2018).

[32] H. Qin, S. J. Hämäläinen, and S. Van Dijken, Exchange-torque-induced excitation of perpendicular standing spin waves in nanometer-thick yig films, *Scientific reports* **8**, 5755 (2018).

[33] Y. Li, W. Cao, V. P. Amin, Z. Zhang, J. Gibbons, J. Sklenar, J. Pearson, P. M. Haney, M. D. Stiles, W. E. Bailey, *et al.*, Coherent spin pumping in a strongly coupled magnon-magnon hybrid system, *Physical review letters* **124**, 117202 (2020).

[34] Y. Li, Z. Zhang, C. Liu, D. Zheng, B. Fang, C. Zhang, A. Chen, Y. Ma, C. Wang, H. Liu, K. Shen, A. Manchon, J. Q. Xiao, Z. Qiu, C.-M. Hu, and X. Zhang, Reconfigurable spin current transmission and magnon-magnon coupling in hybrid ferrimagnetic insulators, *Nat Commun.* **5**, 2234 (2024).

[35] J. Liu, Y. Xiong, J. Liang, X. Wu, C. Liu, S. K. Cheung, Z. Ren, R. Liu, A. Christy, Z. Chen, *et al.*, Strong magnon-magnon coupling and low dissipation rate in an all-magnetic-insulator heterostructure, *Physical Review Applied* **22**, 034017 (2024).

[36] L. Liensberger, A. Kamra, H. Maier-Flaig, S. Geprägs, A. Erb, S. T. B. Goennenwein, R. Gross, W. Belzig, H. Huebl, and M. Weiler, Exchange-enhanced ultra-strong magnon-magnon coupling in a compensated ferrimagnet, *Phys. Rev. Lett.* **123**, 117204 (2019).

[37] D. MacNeill, J. T. Hou, D. R. Klein, P. Zhang, P. Jarillo-Herrero, and L. Liu, Gigahertz frequency antiferromagnetic resonance and strong magnon-magnon coupling in

the layered crystal crcl 3, *Physical review letters* **123**, 047204 (2019).

[38] T. M. J. Cham, S. Karimeddiny, A. H. Dismukes, X. Roy, D. C. Ralph, and Y. K. Luo, Anisotropic gigahertz antiferromagnetic resonances of the easy-axis van der waals antiferromagnet crsbr, *Nano Letters* **22**, 6716 (2022).

[39] G. M. Diederich, J. Cenker, Y. Ren, J. Fonseca, D. G. Chica, Y. J. Bae, X. Zhu, X. Roy, T. Cao, D. Xiao, *et al.*, Tunable interaction between excitons and hybridized magnons in a layered semiconductor, *Nature Nanotechnology* **18**, 23 (2023).

[40] W. Li, Y. Dai, L. Ni, B. Zhang, D. Tang, Y. Yang, and Y. Xu, Ultrastrong magnon–magnon coupling and chirality switching in antiferromagnet crps4, *Advanced Functional Materials* **33**, 2303781 (2023).

[41] T. Makihara, K. Hayashida, G. T. Noe Ii, X. Li, N. Marquez Peraca, X. Ma, Z. Jin, W. Ren, G. Ma, I. Katayama, *et al.*, Ultrastrong magnon–magnon coupling dominated by antiresonant interactions, *Nature communications* **12**, 3115 (2021).

[42] Z. Zhang, F. Y. Gao, Y.-C. Chien, Z.-J. Liu, J. B. Curtiss, E. R. Sung, X. Ma, W. Ren, S. Cao, P. Narang, *et al.*, Terahertz-field-driven magnon upconversion in an antiferromagnet, *Nature Physics* , 1 (2024).

[43] Z. Zhang, F. Y. Gao, J. B. Curtiss, Z.-J. Liu, Y.-C. Chien, A. von Hoegen, M. T. Wong, T. Kurihara, T. Suemoto, P. Narang, *et al.*, Terahertz field-induced nonlinear coupling of two magnon modes in an antiferromagnet, *Nature Physics* , 1 (2024).

[44] J. M. Coey, *Magnetism and magnetic materials* (Cambridge university press, 2010).

[45] M. A. Ruderman and C. Kittel, Indirect exchange coupling of nuclear magnetic moments by conduction electrons, *Physical Review* **96**, 99 (1954).

[46] I. Dzyaloshinsky, A thermodynamic theory of “weak” ferromagnetism of antiferromagnetics, *Journal of physics and chemistry of solids* **4**, 241 (1958).

[47] T. Moriya, Anisotropic superexchange interaction and weak ferromagnetism, *Physical review* **120**, 91 (1960).

[48] J. Chen, T. Yu, C. Liu, T. Liu, M. Madami, K. Shen, J. Zhang, S. Tu, M. S. Alam, K. Xia, *et al.*, Excitation of unidirectional exchange spin waves by a nanoscale magnetic grating, *Physical Review B* **100**, 104427 (2019).

[49] I. Razdolski, A. Alekhin, N. Ilin, J. P. Meyburg, V. Roddatis, D. Diesing, U. Bovensiepen, and A. Melnikov, Nanoscale interface confinement of ultrafast spin transfer torque driving non-uniform spin dynamics, *Nature communications* **8**, 15007 (2017).

[50] L. Brandt, U. Ritzmann, N. Liebing, M. Ribow, I. Razdolski, P. Brouwer, A. Melnikov, and G. Woltersdorf, Effective exchange interaction for terahertz spin waves in iron layers, *Phys. Rev. B* **104**, 094415 (2021).

[51] R. Salikhov, I. Ilyakov, L. Korber, A. Kakay, R. A. Gallardo, A. Ponomaryov, J.-C. Deinert, T. V. de Oliveira, K. Lenz, J. Fassbender, *et al.*, Coupling of terahertz light with nanometre-wavelength magnon modes via spin–orbit torque, *Nature Physics* **19**, 529 (2023).

[52] M. M. Subedi, K. Deng, B. Flebus, and J. Sklenar, Even-odd-layer-dependent symmetry breaking in synthetic antiferromagnets, *Journal of Physics: Condensed Matter* **36**, 375802 (2024).

[53] M. M. Subedi, K. Deng, E. Stimpson, B. Flebus, and J. Sklenar, Investigating the dependence of the bi-quadratic exchange interaction on extrinsic factors in permalloy–ruthenium synthetic antiferromagnets, *Journal of Applied Physics* **137** (2025).

[54] A. H. Comstock, C.-T. Chou, Z. Wang, T. Wang, R. Song, J. Sklenar, A. Amassian, W. Zhang, H. Lu, L. Liu, *et al.*, Hybrid magnonics in hybrid perovskite antiferromagnets, *Nature Communications* **14**, 1834 (2023).

[55] S. Liang, R. Chen, Q. Cui, Y. Zhou, F. Pan, H. Yang, and C. Song, Ruderman–kittel–kasuya–yosida-type interlayer dzyaloshinskii–moriya interaction in synthetic magnets, *Nano Letters* **23**, 8690 (2023).

[56] Y. Wang, Y. Zhang, C. Li, J. Wei, B. He, H. Xu, J. Xia, X. Luo, J. Li, J. Dong, *et al.*, Ultrastrong to nearly deep-strong magnon–magnon coupling with a high degree of freedom in synthetic antiferromagnets, *Nature Communications* **15**, 2077 (2024).

[57] Y. Wang, J. Xia, C. Wan, X. Han, and G. Yu, Ultrastrong magnon–magnon coupling in synthetic antiferromagnets induced by interlayer dzyaloshinskii–moriya interaction, *Physical Review B* **109**, 054416 (2024).

[58] R. Sultana, A. K. Mondal, V. S. Bhat, K. Stenning, Y. Li, D. M. Arroo, A. Vasdev, M. R. McCarter, L. E. De Long, J. T. Hastings, J. C. Gartside, and M. B. Jungfleisch, Ice sculpting: An artificial spin ice Tutorial on controlling microstate and geometry for magnonics and neuromorphic computing, *Journal of Applied Physics* **138**, 061101 (2025).

[59] A. Chumak, A. Serga, and B. Hillebrands, Magnonic crystals for data processing, *Journal of Physics D: Applied Physics* **50**, 244001 (2017).

[60] F. Hellman, A. Hoffmann, Y. Tserkovnyak, G. S. Beach, E. E. Fullerton, C. Leighton, A. H. MacDonald, D. C. Ralph, D. A. Arena, H. A. Dürr, *et al.*, Interface-induced phenomena in magnetism, *Reviews of modern physics* **89**, 025006 (2017).

[61] A. Manchon, J. Železný, I. M. Miron, T. Jungwirth, J. Sinova, A. Thiaville, K. Garello, and P. Gambardella, Current-induced spin-orbit torques in ferromagnetic and antiferromagnetic systems, *Reviews of Modern Physics* **91**, 035004 (2019).

[62] M. Subedi, K. Deng, Y. Xiong, J. Mongeon, M. Hossain, P. Meisenheimer, E. Zhou, J. Heron, M. Jungfleisch, W. Zhang, *et al.*, Engineering antiferromagnetic magnon bands through interlayer spin pumping, *Physical Review Applied* **23**, L031003 (2025).

[63] K. An, M. Xu, A. Mucchietto, C. Kim, K.-W. Moon, C. Hwang, and D. Grundler, Emergent coherent modes in nonlinear magnonic waveguides detected at ultrahigh frequency resolution, *Nature Communications* **15**, 7302 (2024).

[64] H. Pan, Z. An, and C.-M. Hu, Magnon–magnon coupling mediated by topological edge states, *Physical Review Research* **6**, 013020 (2024).

[65] S. Zheng, Z. Wang, Y. Wang, F. Sun, Q. He, P. Yan, and H. Yuan, Tutorial: nonlinear magnonics, *Journal of Applied Physics* **134** (2023).

[66] C. Schönfeld, L. Feuerer, J. Bär, L. Dörfelt, M. Kerstingskötter, T. Dannegger, D. Wuhrer, W. Belzig, U. Nowak, A. Leitenstorfer, *et al.*, Dynamical renormalization of the magnetic excitation spectrum via high-momentum nonlinear magnonics, *Science Advances* **11**, eadv4207 (2025).

[67] Z. Li, J. Sun, and F. Ma, Floquet engineering of selective magnon–magnon coupling in synthetic antiferromagnets, *Applied Physics Letters* **123** (2023).

[68] Y. Fan, T. Fakhrul, J. T. Hou, C.-T. Chou, B. Khrana, Y. Tserkovnyak, L. Liu, and C. A. Ross, Dynamically tunable magnon–magnon coupling in a perpendicular anisotropy magnetic garnet–ferromagnet bilayer, *Physical Review Letters* **134**, 126702 (2025).

[69] D. Schmoll, A. A. Voronov, R. O. Serha, D. Slobodianiuk, K. O. Levchenko, C. Abert, S. Knauer, D. Suess, R. Verba, and A. V. Chumak, Wavenumber-dependent magnetic losses in yttrium iron garnet–gadolinium gallium garnet heterostructures at millikelvin temperatures, *Physical Review B* **111**, 134428 (2025).

[70] R. O. Serha, A. A. Voronov, D. Schmoll, R. Verba, K. O. Levchenko, S. Koraltan, K. Davídková, B. Budinská, Q. Wang, O. V. Dobrovolskiy, *et al.*, Magnetic anisotropy and ggg substrate stray field in yig films down to millikelvin temperatures, *npj Spintronics* **2**, 29 (2024).

[71] J. Wang, H. Wang, J. Chen, W. Legrand, P. Chen, L. Sheng, J. Xia, G. Lan, Y. Zhang, R. Yuan, *et al.*, Broad-wave-vector spin pumping of flat-band magnons, *Physical Review Applied* **21**, 044024 (2024).

[72] J. Sklenar and W. Zhang, Self-hybridization and tunable magnon–magnon coupling in van der waals synthetic magnets, *Physical Review Applied* **15**, 044008 (2021).

[73] H. Wang, W. Legrand, R. Schlitz, and P. Gambardella, Current-controlled magnon–magnon coupling in an on-chip cavity resonator, *Nano Letters* **25**, 9090 (2025).

[74] S. Barman, P. K. Pal, and R. K. Mitra, External control over magnon–magnon coupling in a two-dimensional array of square-shaped nanomagnets, *Advanced Quantum Technologies* , 2500181 (2025).

[75] Q. Wang, G. Csaba, R. Verba, A. V. Chumak, and P. Pirro, Nanoscale magnonic networks, *Physical Review Applied* **21**, 040503 (2024).

[76] A. Sud, K. Yamamoto, S. Iihama, K. Ishibashi, S. Fukami, H. Kurebayashi, and S. Mizukami, Electrically controlled nonlinear magnon–magnon coupling in a synthetic antiferromagnet, *Physical Review Letters* **134**, 246704 (2025).

[77] C. W. Freeman, H. Youel, A. K. Budniak, Z. Xue, H. De Libero, T. Thomson, M. Bosman, G. Eda, H. Kurebayashi, and M. Cubukcu, Tunable ultrastrong magnon–magnon coupling approaching the deep-strong regime in a van der waals antiferromagnet, *ACS nano* **19**, 16024 (2025).

[78] E. Chen, D. Apalkov, Z. Diao, A. Driskill-Smith, D. Druist, D. Lottis, V. Nikitin, X. Tang, S. Watts, S. Wang, S. A. Wolf, A. W. Ghosh, J. W. Lu, S. J. Poon, M. Stan, W. H. Butler, S. Gupta, C. K. A. Mewes, T. Mewes, and P. B. Visscher, Advances and future prospects of spin-transfer torque random access memory, *IEEE Trans. Magn.* **46**, 1873 (2010).

[79] Q. Shao, P. Li, L. Liu, H. Yang, S. Fukami, A. Razavi, H. Wu, K. Wang, F. Freimuth, Y. Mokrousov, M. D. Stiles, S. Emori, A. Hoffmann, J. Åkerman, K. Roy, J.-P. Wang, S.-H. Yang, K. Garello, and W. Zhang, Roadmap of spin–orbit torques, *IEEE Trans. Magn.* **57**, 1 (2021).

[80] A. V. Sadovnikov, A. A. Grachev, S. E. Sheshukova, Y. P. Sharaevskii, A. A. Serdobintsev, D. M. Mitin, and S. A. Nikitov, Magnon straintronics: Reconfigurable spin-wave routing in strain-controlled bilateral magnetic stripes, *Phys. Rev. Lett.* **120**, 257203 (2018).

[81] B. Dai, M. Jackson, Y. Cheng, H. He, Q. Shu, H. Huang, L. Tai, and K. Wang, Review of voltage-controlled magnetic anisotropy and magnetic insulator, *J. Magn. Magn. Mater.* **563**, 169924 (2022).

[82] R. A. Duine, K.-J. Lee, S. S. P. Parkin, and M. D. Stiles, Synthetic antiferromagnetic spintronics, *Nature Physics* **14**, 217 (2018).

[83] J. Lu, W. Deng, X. Huang, M. Ke, and Z. Liu, Non-hermitian topological phononic metamaterials, *Advanced Materials* , 2307998 (2023).

[84] T. Ozawa, H. M. Price, A. Amo, N. Goldman, M. Hafezi, L. Lu, M. C. Rechtsman, D. Schuster, J. Simon, O. Zilbermanberg, and I. Carusotto, Topological photonics, *Reviews of Modern Physics* **91**, 015006 (2019).

[85] H. M. Hurst and B. Flebus, Non-hermitian physics in magnetic systems, *Journal of Applied Physics* **132** (2022).

[86] P. M. Gunnink, B. Flebus, H. M. Hurst, and R. A. Duine, Nonlinear dynamics of the non-hermitian su-schrieffer-heeger model, *Physical Review B* **105**, 104433 (2022).

[87] K. Deng, X. Li, and B. Flebus, Exceptional points as signatures of dynamical magnetic phase transitions, *Physical Review B* **107**, L100402 (2023).

[88] M. Jamali, J. H. Kwon, S.-M. Seo, K.-J. Lee, and H. Yang, Spin wave nonreciprocity for logic device applications, *Scientific reports* **3**, 3160 (2013).

[89] T. Oka and S. Kitamura, Floquet engineering of quantum materials, *Annual Review of Condensed Matter Physics* (2018).

[90] D. Yu, W. Song, L. Wang, R. Srikanth, S. K. Sridhar, T. Chen, C. Huang, G. Li, X. Qiao, X. Wu, *et al.*, A comprehensive review on developments of synthetic dimensions, *arXiv preprint arXiv:2503.01465* (2025).

[91] M. S. Rudner and N. H. Lindner, Band structure engineering and non-equilibrium dynamics in floquet topological insulators, *Nature reviews physics* **2**, 229 (2020).

[92] Y. Li and W. E. Bailey, Wave-number-dependent gilbert damping in metallic ferromagnets, *Phys. Rev. Lett.* **116**, 117602 (2016).

[93] L. Sheng, M. Elyasi, J. Chen, W. He, Y. Wang, H. Wang, H. Feng, Y. Zhang, I. Medlej, S. Liu, *et al.*, Nonlocal detection of interlayer three-magnon coupling, *Physical Review Letters* **130**, 046701 (2023).

[94] H. Qin, R. B. Holländer, L. Flajšman, F. Hermann, R. Dreyer, G. Woltersdorf, and S. van Dijken, Nanoscale magnonic fabry-pérot resonator for low-loss spin-wave manipulation, *Nature communications* **12**, 2293 (2021).

[95] C. Liu, J. Chen, T. Liu, F. Heimbach, H. Yu, Y. Xiao, J. Hu, M. Liu, H. Chang, T. Stueckler, *et al.*, Long-distance propagation of short-wavelength spin waves, *Nature communications* **9**, 738 (2018).

[96] O. A. Santos and B. J. van Wees, Magnon confinement in an all-on-chip yig cavity resonator using hybrid yig/py magnon barriers, *Nano Letters* **23**, 9303 (2023).

[97] Y. Li, C. Zhao, V. P. Amin, Z. Zhang, M. Vogel, Y. Xiong, J. Sklenar, R. Divan, J. Pearson, M. D. Stiles, W. Zhang, A. Hoffmann, and V. Novosad, Phase-resolved electrical detection of coherently coupled magnonic devices, *Appl. Phys. Lett.* **118**, 202403 (2021).

[98] D. Wagle, Y. Li, M. T. Kaffash, S. Lendinez, M. T. Hosain, V. Novosad, and M. B. Jungfleisch, Observation of

thermally activated coherent magnon-magnon coupling in a magnonic hybrid system, *Phys. Rev. B* **112**, 054410 (2025).

[99] B. Hillebrands, Spin-wave calculations for multilayered structures, *Phys. Rev. B* **41**, 530 (1990).

[100] P. Quarterman, Y. Fan, Z. Chen, C. J. Jensen, R. V. Chopdekar, D. A. Gilbert, M. E. Holtz, M. D. Stiles, J. A. Borchers, K. Liu, *et al.*, Probing antiferromagnetic coupling in magnetic insulator/metal heterostructures, *Physical Review Materials* **6**, 094418 (2022).

[101] P. Quarterman, Y. Fan, Z. Chen, C. J. Jensen, R. V. Chopdekar, D. A. Gilbert, M. E. Holtz, M. D. Stiles, J. A. Borchers, K. Liu, L. Liu, and A. J. Grutter, Probing antiferromagnetic coupling in magnetic insulator/metal heterostructures, *Phys. Rev. Mater.* **6**, 094418 (2022).

[102] J. Qian, Y. Li, Z. Jiang, R. Busch, H.-C. Ni, T.-H. Lo, A. Hoffmann, A. Schleife, and J.-M. Zuo, Unraveling the origin of antiferromagnetic coupling at yig/permalloy interface, *Phys. Rev. Mater.* **8**, 104405 (2024).

[103] M. B. Jungfleisch, V. Lauer, R. Neb, A. V. Chumak, and B. Hillebrands, Improvement of the yttrium iron garnet/platinum interface for spin pumping-based applications, *Appl. Phys. Lett.* **103**, 022411 (2013).

[104] Y. Tserkovnyak, A. Brataas, G. E. W. Bauer, and B. I. Halperin, Nonlocal magnetization dynamics in ferromagnetic heterostructures, *Rev. Mod. Phys.* **77**, 1375 (2005).

[105] M. Harder, Y. Yang, B. M. Yao, C. H. Yu, J. W. Rao, Y. S. Gui, R. L. Stamps, and C.-M. Hu, Level attraction due to dissipative magnon-photon coupling, *Phys. Rev. Lett.* **121**, 137203 (2018).

[106] T. M. J. Cham, D. G. Chica, X. Huang, K. Watanabe, T. Taniguchi, X. Roy, Y. K. Luo, and D. C. Ralph, Spin-filter tunneling detection of antiferromagnetic resonance with electrically tunable damping, *Science* **0**, eadq8590 (2025).

[107] Y. J. Bae, J. Wang, A. Scheie, J. Xu, D. G. Chica, G. M. Diederich, J. Cenker, M. E. Ziebel, Y. Bai, H. Ren, *et al.*, Exciton-coupled coherent magnons in a 2d semiconductor, *Nature* **609**, 282 (2022).

[108] M. Fiebig, D. Fröhlich, B. Krichevts, and R. V. Pisarev, Second harmonic generation and magnetic-dipole-electric-dipole interference in antiferromagnetic cr 2 o 3, *Physical Review Letters* **73**, 2127 (1994).

[109] A. Sud, K. Yamamoto, K. Suzuki, S. Mizukami, and H. Kurebayashi, Magnon-magnon coupling in synthetic ferrimagnets, *Physical Review B* **108**, 104407 (2023).

[110] Y. Shiota, T. Taniguchi, M. Ishibashi, T. Moriyama, and T. Ono, Tunable magnon-magnon coupling mediated by dynamic dipolar interaction in synthetic antiferromagnets, *Physical Review Letters* **125**, 017203 (2020).

[111] A. Sud, C. Zollitsch, A. Kämäki, T. Dion, S. Khan, S. Iihama, S. Mizukami, and H. Kurebayashi, Tunable magnon-magnon coupling in synthetic antiferromagnets, *Physical Review B* **102**, 100403 (2020).

[112] C. Dai and F. Ma, Strong magnon-magnon coupling in synthetic antiferromagnets, *Applied Physics Letters* **118** (2021).

[113] M. T. Hossain, H. Chen, S. Bhatt, M. T. Kaffash, J. Q. Xiao, J. Sklenar, and M. B. Jungfleisch, Broken intrinsic symmetry induced magnon-magnon coupling in synthetic ferrimagnets, *arXiv preprint arXiv:2410.06167* (2024).

[114] Y. Rong, C. Jiang, H. Wang, L. Sun, F. Liu, J. Lu, T. Wu, Y. Zhang, Y. Zhao, F. Ma, *et al.*, Layer-dependent magnon-magnon coupling in a synthetic antiferromagnet, *Physical Review Applied* **21**, 054050 (2024).

[115] H. Waring, N. Johansson, I. J. Vera-Marun, and T. Thomson, Zero-field optic mode beyond 20 ghz in a synthetic antiferromagnet, *Physical Review Applied* **13**, 034035 (2020).

[116] A. Zhou, Y. Li, S. Zhang, Z. Jin, W. Guo, F. Xu, X. Wang, D. Cao, J. Xu, G. Zhao, *et al.*, Self-biased optical mode ferromagnetic resonance beyond 22 ghz in artificial exchange coupled trilayers, *Journal of Magnetism and Magnetic Materials* **547**, 168955 (2022).

[117] A. Mouhoub, F. Millo, C. Chappert, J.-V. Kim, J. Lé tang, A. Solignac, and T. Devolder, Exchange energies in cofeb/ru/cofeb synthetic antiferromagnets, *Physical Review Materials* **7**, 044404 (2023).

[118] K. Winther, Z. R. Nunn, J. Lisik, S. Arapan, D. Legut, F. Schulz, E. Goering, T. Mckinnon, S. Myrtle, and E. Girt, Antiferromagnetic coupling across nonmagnetic transition-metal films alloyed with ferromagnetic elements, *Physical Review Applied* **22**, 024058 (2024).

[119] M. Li, J. Lu, and W. He, Symmetry breaking induced magnon-magnon coupling in synthetic antiferromagnets, *Physical Review B* **103**, 064429 (2021).

[120] W. He, Z. Xie, R. Sun, M. Yang, Y. Li, X.-T. Zhao, W. Liu, Z. Zhang, J.-W. Cai, Z.-H. Cheng, *et al.*, Anisotropic magnon-magnon coupling in synthetic antiferromagnets, *Chinese Physics Letters* **38**, 057502 (2021).

[121] Z. Tengfei, W. Quwen, C. Min, D. Jie, Z. Qian, L. Zimu, L. Qingfang, W. Jianbo, and W. Jinwu, Magnon-magnon coupling in noncollinear synthetic antiferromagnets, *Chinese Physics B* (2025).

[122] X. Chen, C. Zheng, H. Xu, and Y. Liu, Micromagnetic simulations of magnon-magnon coupling in synthetic antiferromagnets with tilted magnetic anisotropy, *Journal of Physics: Condensed Matter* (2025).

[123] Y.-H. Huang, X.-W. Lu, J.-H. Han, C.-C. Peng, and C.-F. Pai, Experimental confirmation of ruderman-kittel-kasuya-yosida-type interlayer dzyaloshinskii-moriya interaction across ru spacers, *Physical Review Materials* **9**, L051401 (2025).

[124] H. Qin, R. B. Holländer, L. Flajšman, F. Hermann, R. Dreyer, G. Woltersdorf, and S. van Dijken, Nanoscale magnonic fabry-pérot resonator for low-loss spin-wave manipulation, *Nature Communications* **12**, 10.1038/s41467-021-22520-6 (2021).

[125] A. Talapatra, H. Qin, F. Schulz, L. Yao, L. Flajšman, M. Weigand, S. Wintz, and S. van Dijken, Imaging of short-wavelength spin waves in a nanometer-thick yig/co bilayer, *Applied Physics Letters* 10.1063/5.0149583 (2023).

[126] T. Dion, K. D. Stenning, A. Vanstone, H. H. Holder, R. Sultana, G. Alatteili, V. Martinez, M. T. Kaffash, T. Kimura, R. F. Oulton, *et al.*, Ultrastrong magnon-magnon coupling and chiral spin-texture control in a dipolar 3d multilayered artificial spin-vortex ice, *Nature communications* **15**, 4077 (2024).

[127] G. Gubbiotti, X. Zhou, Z. Haghshenasfard, M. G. Cottam, and A. O. Adeyeye, Reprogrammable magnonic band structure of layered permalloy/cu/permalloy nanowires, *Phys. Rev. B* **97**, 134428 (2018).

[128] S. Lendinez, M. Taghipour Kaffash, and M. B. Jungfleisch, Observation of mode splitting in artificial spin ice: A comparative ferromagnetic resonance and Brillouin light scattering study, *Applied Physics Letters* **118**, 162407 (2021).

[129] J. C. Gartside, A. Vanstone, T. Dion, K. D. Stenning, D. M. Arroo, H. Kurebayashi, and W. R. Branford, Reconfigurable magnonic mode-hybridisation and spectral control in a bicomponent artificial spin ice, *Nature Communications* **12**, 2488 (2021).

[130] F. Montoncello, M. T. Kaffash, H. Carfagno, M. F. Doty, G. Gubbiotti, and M. B. Jungfleisch, A Brillouin light scattering study of the spin-wave magnetic field dependence in a magnetic hybrid system made of an artificial spin-ice structure and a film underlayer, *Journal of Applied Physics* **133**, 083901 (2023).

[131] R. Negrello, F. Montoncello, M. T. Kaffash, M. B. Jungfleisch, and G. Gubbiotti, Dynamic coupling and spin-wave dispersions in a magnetic hybrid system made of an artificial spin-ice structure and an extended NiFe underlayer, *APL Materials* **10**, 091115 (2022).

[132] O. A. Santos and B. J. van Wees, Magnon confinement in an all-on-chip yig cavity resonator using hybrid yig/py magnon barriers, *Nano Letters* **23**, 9303 (2023).

[133] K. G. Fripp, A. V. Shytov, and V. V. Kruglyak, Spin-wave control using dark modes in chiral magnonic resonators, *Physical Review B* **104**, 054437 (2021).

[134] V. S. Bhat and M. B. Jungfleisch, Magnon signatures of multidimensional reconfigurations in multilayer square artificial spin ices, *Applied Physics Letters* **126** (2025).

[135] K. Adhikari, S. Sahoo, A. K. Mondal, Y. Otani, and A. Barman, Large nonlinear ferromagnetic resonance shift and strong magnon-magnon coupling in Ni<sub>80</sub>Fe<sub>20</sub> nanocross array, *Phys. Rev. B* **101**, 054406 (2020).

[136] K. Adhikari, S. Choudhury, S. Barman, Y. Otani, and A. Barman, Observation of magnon-magnon coupling with high cooperativity in ni80fe20 cross-shaped nanoring array, *Nanotechnology* **32**, 395706 (2021).

[137] K. Adhikari, S. Choudhury, S. Barman, Y. Otani, and A. Barman, Observation of magnon-magnon coupling with high cooperativity in ni80fe20 cross-shaped nanoring array, *Nanotechnology* **32**, 395706 (2021).

[138] V. Bhat and D. Grundler, Tuning interactions in reconfigurable kagome artificial spin ices for magnonics, *Applied Physics Letters* **119** (2021).

[139] V. S. Bhat, S. Watanabe, F. Kronast, K. Baumgaertl, and D. Grundler, Spin dynamics, loop formation and cooperative reversal in artificial quasicrystals with tailored exchange coupling, *Communications Physics* **6**, 193 (2023).

[140] M. Saccone, A. Scholl, S. Velten, S. Dhuey, K. Hofhuis, C. Wuth, Y.-L. Huang, Z. Chen, R. V. Chopdekar, and A. Farhan, Towards artificial ising spin glasses: Thermal ordering in randomized arrays of ising-type nanomagnets, *Physical Review B* **99**, 224403 (2019).

[141] P. K. Pal, A. K. Mondal, and A. Barman, Using magnons as a quantum technology platform: a perspective, *Journal of Physics: Condensed Matter* **36**, 441502 (2024).

[142] G. Gubbiotti, A. Barman, S. Ladak, C. Bran, D. Grundler, M. Huth, H. Plank, G. Schmidt, S. Van Dijken, R. Streubel, *et al.*, 2025 roadmap on 3d nanomagnetism, *Journal of Physics: Condensed Matter*.

[143] H. Wang, J. Wang, S. Chen, P. Chen, W. Legrand, Y. Zhang, L. Sheng, R. Yuan, J. Chen, G. Yu, *et al.*, Reconfigurable nonreciprocal excitation of propagating exchange spin waves in perpendicularly magnetized yttrium iron garnet thin films, *Physical Review B* **108**, 134403 (2023).

[144] W. Song, X. Wang, C. Jia, X. Wang, C. Jiang, D. Xue, and G. Chai, Nonreciprocal emergence of hybridized magnons in magnetic thin films, *Physical Review B* **104**, 014402 (2021).

[145] X. Kong, W. Song, C. Li, C. Ong, and G. Chai, Dipolar induced nonreciprocal magnon hybridization in feni/yig bilayers, *Applied Physics Letters* **125** (2024).

[146] M. M. Subedi, K. Deng, Y. Xiong, J. Mongeon, M. T. Hossain, P. Meisenheimer, E. Zhou, J. Heron, M. B. Jungfleisch, W. Zhang, *et al.*, Magnon-magnon interactions induced by spin pumping-driven symmetry breaking in synthetic antiferromagnets, *arXiv preprint arXiv:2301.07311* (2023).

[147] P. M. Levy and A. Fert, Anisotropy induced by non-magnetic impurities in Cu mn spin-glass alloys, *Phys. Rev. B* **23**, 4667 (1981).

[148] A. Fert, V. Cros, and J. Sampaio, Skyrmions on the track, *Nature nanotechnology* **8**, 152 (2013).

[149] Y. Tokura and N. Kanazawa, Magnetic skyrmion materials, *Chemical Reviews* **121**, 2857 (2020).

[150] X. Yu, Y. Onose, N. Kanazawa, J. H. Park, J. Han, Y. Matsui, N. Nagaosa, and Y. Tokura, Real-space observation of a two-dimensional skyrmion crystal, *Nature* **465**, 901 (2010).

[151] X. Yu, N. Kanazawa, Y. Onose, K. Kimoto, W. Zhang, S. Ishiwata, Y. Matsui, and Y. Tokura, Near room-temperature formation of a skyrmion crystal in thin-films of the helimagnet fege, *Nature materials* **10**, 106 (2011).

[152] A. Tonomura, X. Yu, K. Yanagisawa, T. Matsuda, Y. Onose, N. Kanazawa, H. S. Park, and Y. Tokura, Real-space observation of skyrmion lattice in helimagnet mnsi thin samples, *Nano letters* **12**, 1673 (2012).

[153] S. Seki, X. Yu, S. Ishiwata, and Y. Tokura, Observation of skyrmions in a multiferroic material, *Science* **336**, 198 (2012).

[154] R. Wiesendanger, Nanoscale magnetic skyrmions in metallic films and multilayers: a new twist for spintronics, *Nature Reviews Materials* **1**, 1 (2016).

[155] M. R. K. Akanda, I. J. Park, and R. K. Lake, Interfacial dzyaloshinskii-moriya interaction of antiferromagnetic materials, *Phys. Rev. B* **102**, 224414 (2020).

[156] H. Jani, J.-C. Lin, J. Chen, J. Harrison, F. Maccherozzi, J. Schad, S. Prakash, C.-B. Eom, A. Ariando, T. Venkatesan, *et al.*, Antiferromagnetic half-skyrmions and bimerons at room temperature, *Nature* **590**, 74 (2021).

[157] Y. Liang, L. Wu, M. Dai, Y. Zhang, Q. Zhang, J. Wang, N. Zhang, W. Xu, L. Zhao, H. Chen, *et al.*, Significant unconventional anomalous hall effect in heavy metal/antiferromagnetic insulator heterostructures, *Advanced Science* **10**, 2206203 (2023).

[158] S. Ding, A. Ross, R. Lebrun, S. Becker, K. Lee, I. Boventer, S. Das, Y. Kurokawa, S. Gupta, J. Yang, G. Jakob, and M. Kläui, Interfacial dzyaloshinskii-moriya interaction and chiral magnetic textures in a ferrimagnetic insulator, *Phys. Rev. B* **100**, 100406 (2019).

[159] L. Caretta, E. Rosenberg, F. Büttner, T. Fakhrul, P. Gargiani, M. Valvidares, Z. Chen, P. Reddy, D. A. Muller, C. A. Ross, *et al.*, Interfacial dzyaloshinskii-moriya interaction arising from rare-earth orbital magnetism in insulating magnetic oxides, *Nature communications* **11**, 1090 (2020).

[160] A. Fernández-Pacheco, E. Vedmedenko, F. Ummelen, R. Mansell, D. Petit, and R. P. Cowburn, Symmetry-breaking interlayer dzyaloshinskii-moriya interactions in synthetic antiferromagnets, *Nature materials* **18**, 679 (2019).

[161] W. Legrand, D. Maccariello, F. Ajejas, S. Collin, A. Vecchiola, K. Bouzehouane, N. Reyren, V. Cros, and A. Fert, Room-temperature stabilization of antiferromagnetic skyrmions in synthetic antiferromagnets, *Nature materials* **19**, 34 (2020).

[162] H. Y. Yuan, R. Lavrijsen, and R. A. Duine, Unidirectional magnetic coupling induced by chiral interaction and nonlocal damping, *Phys. Rev. B* **107**, 024418 (2023).

[163] Y. Wang, J. Xia, C. Wan, X. Han, and G. Yu, Ultrastrong magnon-magnon coupling in synthetic antiferromagnets induced by interlayer dzyaloshinskii-moriya interaction, *Phys. Rev. B* **109**, 054416 (2024).

[164] L. Cuchet, B. Rodmacq, S. Auffret, R. C. Sousa, I. L. Prejbeanu, and B. Dieny, Perpendicular magnetic tunnel junctions with a synthetic storage or reference layer: A new route towards pt-and pd-free junctions, *Scientific reports* **6**, 21246 (2016).

[165] J.-M. Hu, T. Yang, and L.-Q. Chen, Strain-mediated voltage-controlled switching of magnetic skyrmions in nanostructures, *npj Computational Materials* **4**, 62 (2018).

[166] Z. Zhang, H. Yang, Z. Wang, Y. Cao, and P. Yan, Strong coupling of quantized spin waves in ferromagnetic bilayers, *Phys. Rev. B* **103**, 104420 (2021).

[167] J. Liu, Y. Xiong, J. Liang, X. Wu, C. Liu, S. K. Cheung, Z. Ren, R. Liu, A. Christy, Z. Chen, Y. Liu, F. P. Nugraha, X.-X. Zhang, D. C. W. Leung, W. Zhang, and Q. Shao, Strong magnon-magnon coupling and low dissipation rate in an all-magnetic-insulator heterostructure, *Phys. Rev. Appl.* **22**, 034017 (2024).

[168] S. Rohart and A. Thiaville, Skyrmion confinement in ultrathin film nanostructures in the presence of dzyaloshinskii-moriya interaction, *Phys. Rev. B* **88**, 184422 (2013).

[169] J. Sampaio, V. Cros, S. Rohart, A. Thiaville, and A. Fert, Nucleation, stability and current-induced motion of isolated magnetic skyrmions in nanostructures, *Nature nanotechnology* **8**, 839 (2013).

[170] E. Y. Vedmedenko and M. Kostylev, Boundary conditions for and ferromagnetic resonance spectra of magnetic bilayers coupled by interlayer dzyaloshinskii-moriya interactions, *Phys. Rev. Appl.* **23**, 014047 (2025).

[171] V. Kruglyak, O. Y. Gorobets, Y. I. Gorobets, and A. Kuchko, Magnetization boundary conditions at a ferromagnetic interface of finite thickness, *Journal of Physics: Condensed Matter* **26**, 406001 (2014).

[172] Y. Li, T. Draher, A. H. Comstock, Y. Xiong, M. A. Haque, E. Easy, J. Qian, T. Polakovic, J. E. Pearson, R. Divan, J.-M. Zuo, X. Zhang, U. Welp, W.-K. Kwok, A. Hoffmann, J. M. Luther, M. C. Beard, D. Sun, W. Zhang, and V. Novosad, Probing intrinsic magnon bandgap in a layered hybrid perovskite antiferromagnet by a superconducting resonator, *Phys. Rev. Res.* **5**, 043031 (2023).

[173] P. J. Shah, D. A. Bas, I. Lisenkov, A. Matyushov, N. X. Sun, and M. R. Page, Giant nonreciprocity of surface acoustic waves enabled by the magnetoelastic interaction, *Science advances* **6**, eabc5648 (2020).

[174] O. O. Soykal and M. E. Flatté, Strong field interactions between a nanomagnet and a photonic cavity, *Phys. Rev. Lett.* **104**, 077202 (2010).

[175] Y. Cao, P. Yan, H. Huebl, S. T. B. Goennenwein, and G. E. W. Bauer, Exchange magnon-polaritons in microwave cavities, *Phys. Rev. B* **91**, 094423 (2015).

[176] B. Zare Rameshti, S. Viola Kusminskiy, J. A. Haigh, K. Usami, D. Lachance-Quirion, Y. Nakamura, C.-M. Hu, H. X. Tang, G. E. Bauer, and Y. M. Blanter, Cavity magnonics, *Physics Reports* **979**, 1 (2022).

[177] C. Li, Y. Fan, W. Ding, K. Wang, C. Zhou, D. Song, L. Zhang, Y. Mokrousov, S. Lei, P. Parchinskiy, H. Du, L. Bai, P. Gao, T. Yu, Y.-P. Wang, T. Nan, and P. Li, Probing the spin dynamics of quasi-2d magnets cu(1,3-bdc) using a superconducting resonator, *Applied Physics Letters* **126**, 092407 (2025).

[178] D. Meiser and P. Meystre, Superstrong coupling regime of cavity quantum electrodynamics, *Physical Review A—Atomic, Molecular, and Optical Physics* **74**, 065801 (2006).

[179] S. Shekhar, W. Bogaerts, L. Chrostowski, J. E. Bowers, M. Hochberg, R. Soref, and B. J. Shastri, Roadmapping the next generation of silicon photonics, *Nature Communications* **15**, 751 (2024).

[180] N. Maring, A. Fyrillas, M. Pont, E. Ivanov, P. Stepanov, N. Margaria, W. Hease, A. Pishchagin, A. Lemaître, I. Sagnes, T. H. Au, S. Boissier, E. Bertasi, A. Baert, M. Valdivia, M. Billard, O. Acar, A. Brieussel, R. Mezher, S. C. Wein, A. Salavrakos, P. Sinnott, D. A. Fioretto, P.-E. Emeriau, N. Belabas, S. Mansfield, P. Senellart, J. Senellart, and N. Somaschi, A versatile single-photon-based quantum computing platform, *Nature Photonics* **18**, 603 (2024).

[181] A. Liu, R. Jones, L. Liao, D. Samara-Rubio, D. Rubin, O. Cohen, R. Nicolaescu, and M. Paniccia, A high-speed silicon optical modulator based on a metal-oxide-semiconductor capacitor, *Nature* **427**, 615 (2004).

[182] M. Aspelmeyer, T. J. Kippenberg, and F. Marquardt, Cavity optomechanics, *Rev. Mod. Phys.* **86**, 1391 (2014).

[183] L. Bi, J. Hu, P. Jiang, D. H. Kim, G. F. Dionne, L. C. Kimerling, and C. A. Ross, On-chip optical isolation in monolithically integrated non-reciprocal optical resonators, *Nature Photonics* **5**, 758 (2011).

[184] Y. Zhang, Q. Du, C. Wang, T. Fakhrul, S. Liu, L. Deng, D. Huang, P. Pintus, J. Bowers, C. A. Ross, J. Hu, and L. Bi, Monolithic integration of broadband optical isolators for polarization-diverse silicon photonics, *Optica* **6**, 473 (2019).

[185] K. Srinivasan and B. J. H. Stadler, Review of integrated magneto-optical isolators with rare-earth iron garnets for polarization diverse and magnet-free isolation in silicon photonics, *Opt. Mater. Express* **12**, 697 (2022).

[186] R. Hisatomi, A. Osada, Y. Tabuchi, T. Ishikawa, A. Noguchi, R. Yamazaki, K. Usami, and Y. Nakamura, Bidirectional conversion between microwave and light

via ferromagnetic magnons, *Phys. Rev. B* **93**, 174427 (2016).

[187] M. T. Kaffash, D. Wagle, A. Rai, T. Meyer, J. Q. Xiao, and M. B. Jungfleisch, Direct probing of strong magnon–photon coupling in a planar geometry, *Quantum Science and Technology* **8**, 01LT02 (2022).

[188] A. Osada, R. Hisatomi, A. Noguchi, Y. Tabuchi, R. Yamazaki, K. Usami, M. Sadgrove, R. Yalla, M. Nomura, and Y. Nakamura, Cavity optomagnonics with spin-orbit coupled photons, *Phys. Rev. Lett.* **116**, 223601 (2016).

[189] X. Zhang, N. Zhu, C.-L. Zou, and H. X. Tang, Optomagnonic whispering gallery microresonators, *Phys. Rev. Lett.* **117**, 123605 (2016).

[190] N. Zhu, X. Zhang, X. Han, C.-L. Zou, C. Zhong, C.-H. Wang, L. Jiang, and H. X. Tang, Waveguide cavity optomagnonics for microwave-to-optics conversion, *Optica* **7**, 1291 (2020).

[191] W.-J. Wu, Y.-P. Wang, J. Li, G. Li, and J.-Q. You, Microwave-to-optics conversion using magneto-static modes and a tunable optical cavity, *Laser & Photonics Reviews* **19**, 2400648 (2025).

[192] S. Zhou, Y. Zhu, C. Tang, R. Sun, J. Wu, Y. Xiong, I. E. Russell, Y. Li, D. Sun, F. Tsui, *et al.*, Magneto-optical spectroscopy based on pump-probe strobe light, *Physical Review Applied* **24**, 054061 (2025).

[193] H. Merbouche, B. Divinskiy, D. Goutré, R. Lebrun, A. El Kanj, V. Cros, P. Bortolotti, A. Anane, S. O. Demokritov, and V. E. Demidov, True amplification of spin waves in magnonic nano-waveguides, *Nature Communications* **15**, 1560 (2024).

[194] Y.-Y. Au and K. G. Fripp, Electric field control of chiral magnonic resonators for spin-wave manipulation, *Physical Review Applied* **20**, 034023 (2023).

[195] D. Breitbach, M. Schneider, B. Heinz, F. Kohl, J. Maskill, L. Scheuer, R. O. Serha, T. Brächer, B. Lägel, C. Dubs, *et al.*, Stimulated amplification of propagating spin waves, *Physical Review Letters* **131**, 156701 (2023).

[196] Y. Li, C. Zhao, W. Zhang, A. Hoffmann, and V. Novosad, Advances in coherent coupling between magnons and acoustic phonons, *APL Materials* **9**, 060902 (2021).

[197] J.-M. Hu, Design of new-concept magnetomechanical devices by phase-field simulations, *MRS Bulletin* **49**, 636 (2024).

[198] E. W. Lee, Magnetostriction and magnetomechanical effects, *Reports on progress in physics* **18**, 184 (1955).

[199] V. Vlasov, A. Golov, L. Kotov, V. Shcheglov, A. Lomonosov, and V. Temnov, The modern problems of ultrafast magnetoacoustics, *Acoustical Physics* **68**, 18 (2022).

[200] B. Casals, N. Statuto, M. Foerster, A. Hernández-Mínguez, R. Cicheler, P. Manshausen, A. Mandziak, L. Aballe, J. M. Hernández, and F. Macià, Generation and imaging of magnetoacoustic waves over millimeter distances, *Phys. Rev. Lett.* **124**, 137202 (2020).

[201] M. Bombeck, A. S. Salasyuk, B. A. Glavin, A. V. Scherbakov, C. Brüggemann, D. R. Yakovlev, V. F. Sapega, X. Liu, J. K. Furdyna, A. V. Akimov, and M. Bayer, Excitation of spin waves in ferromagnetic (ga,mn)as layers by picosecond strain pulses, *Phys. Rev. B* **85**, 195324 (2012).

[202] L. Thevenard, E. Peronne, C. Gourdon, C. Testelin, M. Cubukcu, E. Charron, S. Vincent, A. Lemaître, and B. Perrin, Effect of picosecond strain pulses on thin layers of the ferromagnetic semiconductor (ga,mn)(as,p), *Phys. Rev. B* **82**, 104422 (2010).

[203] A. Ghita, T.-G. Mocioi, A. M. Lomonosov, J. Kim, O. Kovalenko, P. Vavassori, and V. V. Temnov, Anatomy of ultrafast quantitative magnetoacoustics in freestanding nickel thin films, *Phys. Rev. B* **107**, 134419 (2023).

[204] T.-G. Mocioi, A. Ghita, and V. V. Temnov, Towards resonantly enhanced acoustic phonon-exchange magnon interactions at thz frequencies, *Magnetochemistry* **9**, 184 (2023).

[205] U. Vernik, A. M. Lomonosov, V. S. Vlasov, L. N. Kotov, D. A. Kuzmin, I. V. Bychkov, P. Vavassori, and V. V. Temnov, Resonant phonon-magnon interactions in free-standing metal-ferromagnet multilayer structures, *Phys. Rev. B* **106**, 144420 (2022).

[206] K. An, A. N. Litvinenko, R. Kohno, A. A. Fuad, V. V. Naletov, L. Vila, U. Ebels, G. de Loubens, H. Hurd-equint, N. Beaulieu, J. Ben Youssef, N. Vukadinovic, G. E. W. Bauer, A. N. Slavin, V. S. Tiberkevich, and O. Klein, Coherent long-range transfer of angular momentum between magnon kittel modes by phonons, *Phys. Rev. B* **101**, 060407 (2020).

[207] J. Xu, C. Zhong, X. Zhou, X. Han, D. Jin, S. K. Gray, L. Jiang, and X. Zhang, Coherent pulse echo in hybrid magnonics with multimode phonons, *Phys. Rev. Appl.* **16**, 024009 (2021).

[208] S. Zhuang, P. B. Meisenheimer, J. Heron, and J.-M. Hu, A narrowband spintronic terahertz emitter based on magnetoelastic heterostructures, *ACS Applied Materials & Interfaces* **13**, 48997 (2021).

[209] S. Zhuang and J.-M. Hu, Excitation and detection of coherent sub-terahertz magnons in ferromagnetic and antiferromagnetic heterostructures, *npj Computational Materials* **8**, 167 (2022).

[210] S. Zhuang and J.-M. Hu, Acoustic attenuation in magnetic insulator films: effects of magnon polaron formation, *Journal of Physics D: Applied Physics* **56**, 054004 (2023).

[211] S. Zhuang, X. Zhang, Y. Zhu, N. X. Sun, C.-B. Eom, P. G. Evans, and J.-M. Hu, Hybrid magnon-phonon cavity for large-amplitude terahertz spin-wave excitation, *Phys. Rev. Appl.* **21**, 044009 (2024).

[212] O. Matsuda, M. C. Larciprete, R. L. Voti, and O. B. Wright, Fundamentals of picosecond laser ultrasonics, *Ultrasonics* **56**, 3 (2015).

[213] Hu, Jiamian and Zhuang, Shihao, Narrowband, acoustically mediated spintronic terahertz emitter (US11112355B2), granted September 7, 2021.

[214] Hu, Jiamian and Zhuang, Shihao, Single-mode, high-frequency, high-power narrowband spintronic terahertz emitter (US11199447B1), granted December 14, 2021.

[215] Hu, Jiamian and Zhuang, Shihao and Li, Mingrui, Magnonic electromagnetic radiation sources with high output power at high frequencies (US11817242B2), granted November 14, 2023.

[216] Hu, Jiamian and Zhuang, Shihao and Eom, Chang-Beom, Magnetic-field-tunable terahertz optoelectronic transducer (US12345930B2), granted July 1, 2025.

[217] J. Liu, Y. Xiong, J. Liang, X. Wu, C. Liu, S. K. Cheung, Z. Ren, R. Liu, A. Christy, Z. Chen, Y. Liu, F. P.

Nugraha, X.-X. Zhang, D. C. W. Leung, W. Zhang, and Q. Shao, Strong magnon-magnon coupling and low dissipation rate in an all-magnetic-insulator heterostructure, *Phys. Rev. Appl.* **22**, 034017 (2024).

[218] B. Khurana, A. C. Kaczmarek, C.-T. Chou, T. Su, K. Lasinger, T. Grossmark, D. C. Bono, L. Liu, and C. A. Ross, Rare-earth iron garnet superlattices with sub-unit cell composition modulation, *ACS nano* **18**, 35269 (2024).

[219] S. Das, R. Mansell, L. Flajšman, L. Yao, and S. Van Dijken, Perpendicular magnetic anisotropy in bi-substituted yttrium iron garnet films, *Journal of Applied Physics* **134** (2023).

[220] J. Ding, C. Liu, Y. Zhang, U. Erugu, Z. Quan, R. Yu, E. McCollum, S. Mo, S. Yang, H. Ding, X. Xu, J. Tang, X. Yang, and M. Wu, Nanometer-thick yttrium iron garnet films with perpendicular anisotropy and low damping, *Phys. Rev. Appl.* **14**, 014017 (2020).

[221] Y. Fan, T. Fakhrul, J. T. Hou, C.-T. Chou, B. Khurana, Y. Tserkovnyak, L. Liu, and C. A. Ross, Dynamically tunable magnon-magnon coupling in a perpendicular anisotropy magnetic garnet-ferromagnet bilayer, *Phys. Rev. Lett.* **134**, 126702 (2025).

[222] F. Dirnberger, J. Quan, R. Bushati, G. M. Diederich, M. Florian, J. Klein, K. Mosina, Z. Sofer, X. Xu, A. Kamra, *et al.*, Magneto-optics in a van der waals magnet tuned by self-hybridized polaritons, *Nature* **620**, 533 (2023).

[223] Y. Sun, F. Meng, C. Lee, A. Soll, H. Zhang, R. Ramesh, J. Yao, Z. Sofer, and J. Orenstein, Dipolar spin wave packet transport in a van der waals antiferromagnet, *Nature Physics* **20**, 794 (2024).

[224] J. Cenker, S. Sivakumar, K. Xie, A. Miller, P. Thijssen, Z. Liu, A. Dismukes, J. Fonseca, E. Anderson, X. Zhu, *et al.*, Reversible strain-induced magnetic phase transition in a van der waals magnet, *Nature Nanotechnology* **17**, 256 (2022).

[225] G. M. Diederich, J. Cenker, Y. Ren, J. Fonseca, D. G. Chica, Y. J. Bae, X. Zhu, X. Roy, T. Cao, D. Xiao, and X. Xu, Tunable interaction between excitons and hybridized magnons in a layered semiconductor, *Nature Nanotechnology* **18**, 23 (2023).

[226] G. M. Diederich, M. Nguyen, J. Cenker, J. Fonseca, S. Pumulo, Y. J. Bae, D. G. Chica, X. Roy, X. Zhu, D. Xiao, Y. Ren, and X. Xu, Exciton dressing by extreme nonlinear magnons in a layered semiconductor, *Nature Nanotechnology* **20**, 617 (2025).

[227] N. P. Wilson, K. Lee, J. Cenker, K. Xie, A. H. Dismukes, E. J. Telford, J. Fonseca, S. Sivakumar, C. Dean, T. Cao, *et al.*, Interlayer electronic coupling on demand in a 2d magnetic semiconductor, *Nature Materials* **20**, 1657 (2021).

[228] M. Wu, Z. Li, T. Cao, and S. G. Louie, Physical origin of giant excitonic and magneto-optical responses in two-dimensional ferromagnetic insulators, *Nature communications* **10**, 2371 (2019).

[229] F. Dirnberger, R. Bushati, B. Datta, A. Kumar, A. H. MacDonald, E. Baldini, and V. M. Menon, Spin-correlated exciton-polaritons in a van der waals magnet, *Nature Nanotechnology* **17**, 1060 (2022).

[230] N. J. Brennan, C. A. Noble, J. Tang, M. E. Ziebel, and Y. J. Bae, Important elements of spin-exciton and magnon-exciton coupling, *ACS Physical Chemistry Au* **4**, 322 (2024).

[231] Y. J. Bae, T. Handa, Y. Dai, J. Wang, H. Liu, A. Scheie, D. G. Chica, M. E. Ziebel, A. D. Kent, X. Xu, K. Shen, X. Roy, and X. Zhu, Transient magnetoelastic coupling in crsbr, *Phys. Rev. B* **109**, 104401 (2024).

[232] P. Gu, Y. Sun, C. Wang, Y. Peng, Y. Zhu, X. Cheng, K. Yuan, C. Lyu, X. Liu, Q. Tan, Q. Zhang, L. Gu, Z. Wang, H. Wang, Z. Han, K. Watanabe, T. Taniguchi, J. Yang, J. Zhang, W. Ji, P.-H. Tan, and Y. Ye, Magnetic phase transitions and magnetoelastic coupling in a two-dimensional stripy antiferromagnet, *Nano Lett.* **22**, 1233 (2022).

[233] J. Xu, C. Zhong, X. Han, D. Jin, L. Jiang, and X. Zhang, Floquet cavity electromagnonics, *Phys. Rev. Lett.* **125**, 237201 (2020).

[234] A. Pishehvar, Z. Wang, Y. Zhu, Y. Jiang, Z. Yan, F. Li, J. M. Jornet, J.-M. Hu, L. Jiang, and X. Zhang, On-demand magnon resonance isolation in cavity magnonics, *Phys. Rev. Appl.* **23**, 024053 (2025).

[235] I. Martin, G. Refael, and B. Halperin, Topological frequency conversion in strongly driven quantum systems, *Physical Review X* **7**, 041008 (2017).

[236] J. Xu, C. Zhong, X. Han, D. Jin, L. Jiang, and X. Zhang, Floquet cavity electromagnonics, *Physical Review Letters* **125**, 237201 (2020).

[237] Y. Yang, Y. Xiao, and C.-M. Hu, Theory of floquet-driven dissipative cavity magnonics, *Physical Review B* **107**, 054413 (2023).

[238] W. Liu, Q. Liu, X. Ni, Y. Jia, K. Ziegler, A. Alù, and F. Chen, Floquet parity-time symmetry in integrated photonics, *Nature Communications* **15**, 946 (2024).

[239] F.-Y. Zhang, Q.-C. Wu, and C.-P. Yang, Non-hermitian shortcut to adiabaticity in floquet cavity electromagnonics, *Physical Review A* **106**, 012609 (2022).

[240] S. Gliga, E. Iacocca, and O. G. Heinonen, Dynamics of reconfigurable artificial spin ice: Toward magnonic functional materials, *APL Materials* **8** (2020).

[241] J. Sklenar, S. Lendinez, and M. B. Jungfleisch, Dynamics in artificial spin ice and magnetic metamaterials, in *Solid State Physics*, Vol. 70 (Elsevier, 2019) pp. 171–235.

[242] S. H. Skjærvø, C. H. Marrows, R. L. Stamps, and L. J. Heyderman, Advances in artificial spin ice, *Nature Reviews Physics* **2**, 13 (2020).

[243] J. R. Wang, C. Nisoli, R. Freitas, J. Li, W. McConville, B. Cooley, M. Lund, N. Samarth, C. Leighton, V. Crespi, *et al.*, Artificial ‘spin ice’ in a geometrically frustrated lattice of nanoscale ferromagnetic islands, *Nature* **439**, 303 (2006).

[244] S. H. Skjærvø, C. H. Marrows, R. L. Stamps, and L. J. Heyderman, Advances in artificial spin ice, *Nature Reviews Physics* **2**, 13 (2020).

[245] S. Lendinez and M. B. Jungfleisch, Magnetization dynamics in artificial spin ice, *J. Phys.: Condens. Matter* **32**, 013001 (2020).

[246] S. Gliga, E. Iacocca, and O. G. Heinonen, Dynamics of reconfigurable artificial spin ice: Toward magnonic functional materials, *APL Materials* **8**, 040911 (2020).

[247] J. C. Gartside, K. D. Stenning, A. Vanstone, H. H. Holder, D. M. Arroo, T. Dion, F. Caravelli, H. Kurebayashi, and W. R. Branford, Reconfigurable training and reservoir computing in an artificial spin-vortex ice via spin-wave fingerprinting, *Nature Nanotechnology* **17**, 460 (2022).

- [248] A. Vanstone, J. C. Gartside, K. D. Stenning, T. Dion, D. M. Arroo, and W. R. Branford, Spectral fingerprinting: microstate readout via remanence ferromagnetic resonance in artificial spin ice, *New Journal of Physics* **24**, 043017 (2022).
- [249] K. D. Stenning, J. C. Gartside, L. Manneschi, C. T. S. Cheung, T. Chen, A. Vanstone, J. Love, H. Holder, F. Caravelli, H. Kurebayashi, K. Everschor-Sitte, E. Vasilaki, and W. R. Branford, Neuromorphic overparameterisation and few-shot learning in multilayer physical neural networks, *Nature Communications* **15**, 7377 (2024).
- [250] M. J. Harris, S. Bramwell, D. McMorrow, T. Zeiske, and K. Godfrey, Geometrical frustration in the ferromagnetic pyrochlore  $Ho_2Ti_{207}$ , *Physical Review Letters* **79**, 2554 (1997).
- [251] S. T. Bramwell and M. J. Gingras, Spin ice state in frustrated magnetic pyrochlore materials, *Science* **294**, 1495 (2001).
- [252] B. Rana, A. K. Mondal, S. Bandyopadhyay, and A. Barman, Applications of nanomagnets as dynamical systems: II, *Nanotechnology* **33**, 082002 (2021).
- [253] S. Lendinez and M. Jungfleisch, Magnetization dynamics in artificial spin ice, *Journal of Physics: Condensed Matter* **32**, 013001 (2019).
- [254] G. Gubbiotti, A. Barman, S. Ladak, C. Bran, D. Grundler, M. Huth, H. Plank, G. Schmidt, S. van Dijken, R. Streubel, *et al.*, 2025 roadmap on 3d nanomagnetism, *Journal of Physics: Condensed Matter* (2024).
- [255] A. Barman, G. Gubbiotti, S. Ladak, A. O. Adeyeye, M. Krawczyk, J. Gräfe, C. Adelmann, S. Cotofana, A. Naeemi, V. I. Vasyuchka, *et al.*, The 2021 magnonics roadmap, *Journal of Physics: Condensed Matter* **33**, 413001 (2021).
- [256] M. T. Kaffash, S. Lendinez, and M. B. Jungfleisch, Nanomagnonics with artificial spin ice, *Physics Letters A* **402**, 127364 (2021).
- [257] S. Ladak, A. Fernández-Pacheco, and P. Fischer, Science and technology of 3d magnetic nanostructures, *APL Materials* **10**, 120401 (2022).
- [258] A. Fernández-Pacheco, R. Streubel, O. Fruchart, R. Hertel, P. Fischer, and R. P. Cowburn, Three-dimensional nanomagnetism, *Nature Communications* **8**, 15756 (2017).
- [259] A. F. Kockum, A. Miranowicz, S. De Liberato, S. Savasta, and F. Nori, Ultrastrong coupling between light and matter, *Nature Reviews Physics* **1**, 19 (2019).
- [260] P. Pirro, V. I. Vasyuchka, A. A. Serga, and B. Hillebrands, Advances in coherent magnonics, *Nature Reviews Materials* **6**, 1114 (2021).
- [261] A. May, M. Saccone, A. van den Berg, J. Askey, M. Hunt, and S. Ladak, Magnetic charge propagation upon a 3d artificial spin-ice, *Nature Communications* **12**, 3217 (2021).
- [262] M. Saccone, A. Van den Berg, E. Harding, S. Singh, S. R. Giblin, F. Flicker, and S. Ladak, Exploring the phase diagram of 3d artificial spin-ice, *Communications Physics* **6**, 217 (2023).

## FIGURE LEGENDS

**Figure 1.** The field of hybrid magnonics has grown and developed into different ramifications, such as magnon-photon, magnon-phonon, and magnon-light coupling systems, with the goal of developing energy and signal transduction functionalities across different physical platforms. The magnon-magnon coupling is presented as a unique and versatile approach towards inducing and tailoring magnon modes with desirable properties for further hybridization in the various hybrid magnonic contexts, i.e. Magnon +  $X$ . In an analogous Bloch sphere representation, the “magnonic Ramsey process” incurs two  $\pi/2$ -pulses that prompt a non-interaction zone and open a free-precession regime between the two-level states, enabling the magnon phase as a state control variable, in contrast to the Rabi process, which only shuffles states directly between the two interaction zones.

**Figure 2.** The various key attributes of magnon-magnon coupling in the context of hybrid magnonics.

**Figure 3.** (a) Schematic of coupled magnon-magnon dynamics in a YIG/FM bilayer mediated by interfacial exchange coupling, with uniform mode ( $k = 0$ ) excited in the FM layer and the perpendicular standing spin wave mode ( $k > 0$ ) excited in the YIG layer. (b)  $H_r$ - $\omega$  dependence for the YIG PSSW mode (red) and the FM uniform mode (blue) that intersect with each other. YIG uniform mode is also shown in red dashed curve. (c-f) Coherent magnon-magnon coupling in (c) YIG/Co [30], (d) YIG/Ni[31], (e) YIG/CoFeB[32] and (f) YIG/NiFe[33].

**Figure 4.** The various geometries of magnon-magnon coupling in bilayer magnetic heterostructures. (a,b,c): uniform, extended bilayer coupling in which the thickness of the film defines the magnonic cavity, for (b) insulator/metal (Figure taken from Ref.[15]), and (c) all-insulator systems (Figure taken from Ref. [35]). (d,e,f): the device geometry in which an FM stripe couples locally to an extended YIG film. The excited magnons can propagate along the lateral dimension, and be detected via: (e) dc rectifications, e.g., using spin Hall effect of Pt (Figure taken from Ref. [93]), or (f) with rf inductive antennas and magneto-optical probes (Figure taken from Ref. [94]). (g,h,i): lateral magnonic cavity in which the FM stripes (h) serve as complementary, local antennas (Figure taken from Ref. [95]), or (i) only used to define the cavity boundaries while the excitation is globally sourced otherwise (Figure taken from Ref. [96]).

**Figure 5.** Detecting magnon-magnon coupling in 2D AFM systems. (a) Schematic of microwave absorption experiment with 2D material. (b) Right-handed (RH) and left-handed (LH) magnon modes. (c) Optical and acoustic magnon modes. (d) Strong magnon-magnon coupling between RH and LH modes in CrSBr. (e) Strong magnon-magnon coupling between optical and acoustic modes in  $CrCl_3$ . The coupling is only activated by breaking in-plane rotational symmetry. (f) Magnetic state alters the exciton resonance energy in CrSBr. (g) Bright and dark magnon modes. (h) Magnon dispersion de-

tected with optical reflectivity measurements in CrSBr. (i) Calculated transient exciton resonance energy shift from the optical (red) and acoustic (blue) magnon modes. (j) Coherent magnon hybridization between bright and dark magnon modes detected by time-resolved measurement. (Figures (a-d) taken from Ref. [38]; (e) taken from Ref. [37]; (f-j) taken from Ref. [39].)

**Figure 6.** Detecting magnon-magnon coupling in bulk AFM systems. (a) Schematic of time-resolved THz free induction decay (FID) measurement. (b) Sample geometry of  $\text{YFeO}_3$  in a tilted magnetic field to study the THz frequency magnon bands. (c) Calculated co-rotating (blue) and counter-rotating (red) coupling strengths show the dominance of the counter-rotating coupling terms. (d) Measured THz magnon bands and the ultra-strong magnon-magnon coupling in  $\text{YFeO}_3$ . (e) quasi-FM (qFM) and quasi-AFM (qAFM) magnon mode. (f) Excitation of different magnon modes in  $\text{ErFeO}_3$ . (g) Strong magnon frequency up-conversion illustrated in 2D THz FID spectra. (h) Dependence of the magnon up-conversion signal amplitude on the pump magnetic field. (i) Magnon energy-level diagrams. (j) The 2D THz spectra in  $\text{YFeO}_3$  summarizing the rich linear and non-linear processes including pump-probe (PP), rephasing or photon echo (R), non-rephasing (NR), two-quantum (2Q), second harmonic generation (SHG), sum-frequency generation (SFG) and difference frequency generation (DFG). (Figures (a),(e),(i),(j) taken from Ref. [43]; (b-d) taken from Ref. [41]; (f-h) taken from Ref. [42].)

**Figure 7.** Interactions between acoustic and optical magnons in synthetic magnets are summarized above. The upper left portion of the figure illustrates how, for synthetic antiferromagnets, the crossing between an acoustic and optical branch [(a)] can turn into an avoided crossing by changing the wave number [(b)], or applying a symmetry breaking external field oblique to the sample plane, [(c), (d)]. The respective references for these images are taken from [109], [110], [111], and [112]. Similar avoided crossings are shown in the lower left portion of the figure in a synthetic ferrimagnet, where the magnetic layers have unequal thicknesses or dissimilar magnetizations, [(e), (f)] taken from Ref. [109, 113]. An alternative

strateggy to engineer interactions into these materials is by changing the number of magnetic layers. The right portion of the figure, [(g), (h)] taken from Ref. [62, 114], shows how in a tetralayer, acoustic or optical magnon pairs interact. If interlayer spin pumping is present in the tetralayer, optical and acoustic magnon pairs can interact as well without the aid of a symmetry breaking field.

**Figure 8.** (a), (b) Phase-resolved TR-MOKE microscopy maps and line profiles measured on a 100-nm-thick  $\text{Y}_3\text{Fe}_5\text{O}_{12}$  (YIG) film with a 730-nm-wide CoFeB stripe. Figure taken from ref. [124]. (c) High-resolution normalized TR-STXM images and line profiles of propagating short-wavelength spin waves in the YIG/Co bilayer at 2.36 GHz with a 10 mT bias field. Figure taken from ref. [125]. (d) Ferromagnetic resonance (FMR) spectra for parallel (black) and antiparallel (red) macrospin states, showing a 1 GHz frequency shift between the states at  $H_{\text{ext}} = 0$ . An SEM schematic defines the DC external field  $H_{\text{ext}}$  and RF field  $H_{\text{RF}}$  orientations for the FMR data panels in this figure. Figure taken from ref. [126]. (e) Schematic of the proposed all-on-chip device inspired by previous studies on dynamic dipolar coupling. The  $\text{Ni}_{81}\text{Fe}_{19}$  (blue), Penrose P3 nanomagnet arrays (maroon), and Pt (gray) are patterned on plain YIG (dark green). The entire chip is placed on an RF co-planar waveguide (CPW). A global spin-pumping voltage can be determined by connecting a nanovoltmeter to the Pt stripes, whereas the local mode profile can be obtained using BLS methods (bright green indicating the laser).

**Figure 9.** Future perspective of magnon-magnon coupling as an approach to modulate interactions in other hybrid magnonic systems. Examples including (top to bottom): (a) tuning magnon-photon interaction via magnon-magnon gap, figure taken from Ref. [172]; (b) modulating magnon-light interaction and spectrum using magneto-optical effect and its inverse, figure taken from Ref. [18]; (c) synergy with magnon-exciton modulation, figure taken from Ref. [107]; (d) nonreciprocal magnon-phonon interaction due to magnon-magnon coupling, figure taken from Ref. [173]; (e) artificial spin ice system leveraging magnon-magnon coupling, figure taken from Ref. [126].